Challenge Journal of STRUCTURAL MECHANICS

Vol.10 No.3 (2024)

auxetic buckling load building codes
compressive strength dynamic analysis
earthquake finite element method
girder bridge Jaya algorithm metaheuristic
algorithms modal analysis optimization
prestresing pushover analysis reinforced
concrete seismic design shallow foundations
smart concrete stability static analysis
steel structures structural dynamics
temperature effects thick plate wind

ISSN 2149-8024

TULPAR ACADEMIC PUBLISHING

Challenge Journal of Structural Mechanics

E-mail: *cjsmec@challengejournal.com*

Web page: *cjsmec.challengejournal.com*

Tulpar Academic Publishing
www.tulparpublishing.com

Challenge Journal of Structural Mechanics

CONTENTS

Research Articles

TULPAR ACADEMIC PUBLISHING

Challenge Journal of Structural Mechanics

Research Article

Prediction of optimum design of welded beam design via machine learning

Yaren Aydın [a], Farnaz Ahadian [a], Gebrail Bekdaş [a], Sinan Melih Nigdeli [a,*]

[a] *Department of Civil Engineering, İstanbul University-Cerrahpaşa, 34320 İstanbul, Türkiye*

ABSTRACT

Design optimization is an important engineering design topic. One of the important issues in structural design is to minimize the cost. This study based on an engineering problem of Welded Beam Design aims to minimize the cost of the beam with machine learning (ML) models depending on the constraints on applied load, shear stress, bending stress and end deflection. The data set to be used in this context was created using a metaheuristic optimization algorithm. This hybrid algorithm is based on the classical Jaya algorithm by adding the student phase of Teaching Learning Based Optimization. The dataset obtained as a result of the optimization is a dataset with 1189 rows. Six different algorithms were used for prediction analyses. These are Linear Regression, Decision Tree, Elastic Net, K-Nearest Neighbour, Random Forest, and XGBoost algorithm. In the data set, load, length, and displacement are input; the design variables such as *b*, *h*, *l*, *t* and minimum cost are output. Since there is more than one output in the dataset, Multioutput Regression is applied. The performance of regression models was assessed using the Coefficient of Determination (R^2), Mean Absolute Error (MAE), and Root Mean Square Error (RMSE). According to the results obtained, the Decision Tree Model showed the best performance among the other models (R^2=1, MAE=6.13e-11, RMSE=9.47e-10).

ARTICLE INFO

Article history:
Received 21 March 2024
Revised 18 April 2024
Accepted 30 April 2024

Keywords:
Welded beam
Multioutput regression
Optimization
Machine learning
Minimum cost

1. Introduction

Optimization is the process of finding the optimum solution to obtain the best value of the objective function. Structural optimization is a type of optimization in which the best of the available options in structural design is sought. There are many studies in the literature where structural optimization and machine learning (ML) are performed using algorithms. In engineering optimization, the problem is generally nonlinear because there are design variables and design constraints on the analysis results that require the design of all variables. In that case, a numerical optimization technique is used that uses iterations with randomly defined candidate solutions to try out the best result. Due to these factors, when an optimization problem cannot be solved using mathematical methods, a systematic methodology is required. This need can be achieved by employing metaheuristic techniques. In metaheuristic methods, the essential problem is formulated in an optimization phase that generates updated candidate design variables. Bekdaş and Nigdeli (2011) used Harmony search (HS) to obtain the optimum parameters of tuned mass dampers (TMD) used for structural control. Thus, more efficient structural control can be achieved with optimum parameter values. Bekdaş (2014) used the harmony search algorithm for the economic design of post-tensioned axisymmetric cylindrical reinforced concrete (RC) walls according to ACI 318. The results showed that the optimization performed with the HS algorithm was effective in the optimum design of the post-tensioned reinforced concrete walls considered in the study. Bekdaş et al. (2015) aimed to minimize the weight of truss structures using the flower pollination algorithm (FPA). The weight obtained with FPA was also optimized compared to other methods. Bekdaş and Nigdeli (2016) carried out

* *Corresponding author*. Tel.: +90-212-473-7070 ; E-mail address: melihnig@iuc.edu.tr (S. M. Nigdeli)
ISSN: 2149-8024 / DOI: https://doi.org/10.20528/cjsmec.2024.03.001

the cost optimization of reinforced concrete elements considering the ACI 318 code by using the bat algorithm. The method used has shown effective success compared to other methods. Kayabekir et al. (2018) performed the optimum design of carbon fiber-reinforced polymer strips used to increase the shear capacity of a reinforced concrete beam using the Jaya algorithm. As a result, Jaya algorithm, which is easy to apply in terms of phase, has been successful in the optimization process. Ulusoy et al. (2019) optimized the proportional gain, integral time and derivative time, which are the optimum parameters of Proportional-Derivative-Integral (PID) type controllers for active control of structures, using the Teaching Learning-Based Optimization (TLBO) algorithm and achieved effective results. Ulusoy et al. (2020) used meta-heuristic algorithms such as Harmony Search, Bat Algorithm and Teaching Learning-Based Optimization for cost minimization of reinforced concrete beams and achieved optimum results.

In recent years, machine learning (ML) has emerged as a promising tool for tackling optimization problems. ML techniques offer the ability to learn patterns and relationships from data, enabling the estimation of complex functions without explicitly modeling them. This capability has led to the development of innovative approaches for estimating and solving optimization problems. Huang et al. (2012) undertook research focusing on hazard identification within smart buildings employing machine learning (ML) methods. They devised an ML algorithm capable of analyzing data gathered from sensors to autonomously issue timely warning alerts for identified hazards. The experimental findings confirmed the efficacy of the ML algorithm and demonstrated the benefits of employing a wireless sensor network for prompt hazard detection in buildings. Jeon et al. (2014) presented statistical models for the shear strength of column-beam connections using BC techniques. The multiple linear regression method was used in the study. It has been observed that this method is applicable for evaluating the joint zone capacity in existing frame-type reinforced concrete buildings. Doğan (2018) tried to determine the post-earthquake damage levels of reinforced concrete columns with a smart system-based method. Data sets were created with the help of 390 damaged images taken from column surfaces. The characteristics of the cracks were extracted from the damage images and the damage level of the columns was classified using ML classifier algorithms according to these data. The successes obtained from the predictions vary between 64% and 80%. Okazaki et al. (2020) conducted a study on the applicability of ML to crack modeling in concrete bridges. The results showed excellent applicability of ML even for very little data. Cao et al. (2020) used ML methods to estimate moments for column-beam connections. The accuracy of the predicted prediction was compared with Artificial Neural Networks and Genetic Programming (GP) and the results showed that ML algorithms provided better performance. Yücel et al. (2021) obtained data by optimization process to be used in machine learning for prediction in reinforced concrete elements. As a result, they achieved successful application. Cakiroglu et al. (2021) minimized the CO_2 emission and cost of steel tube columns filled with concrete. Thus, they optimally dimensioned the cross-sections of the columns. Yücel et al. (2021) estimated the optimum dimensions of reinforced concrete (RC) cantilever retaining walls using metaheuristic algorithms and artificial intelligence and machine learning methods. Successful results were obtained for estimation in the study. Bekdaş et al. (2022) estimated the wall thickness of a cylindrical water tank using HS optimization algorithm using a data set consisting of a large number of optimum design values. The ML models used in the study achieved high success in prediction. Bekdaş et al. (2022) generated data for the optimal sizing of reinforced concrete circular columns using the adaptive search algorithm and used it for prediction in machine learning. Thus, they established a highly efficient estimation procedure. Aydın et al. (2023a) used machine learning models to estimate the cooling load of buildings in hot locations. In the study, Histogram Gradient Boosting and Stacking models were used with high success. Aydın et al. (2023b) performed soil classification using machine learning. As a result of this study in which they processed the data with different processes, boosting models had high performance. Aydın et al. (2023c) applied meta-heuristic optimization algorithms and neural network models to minimize environmental damage in cement production. In the study, the hyperparameter optimization algorithm achieved the highest success with the genetic algorithm (GA). Aydin et al. (2024a) investigated the optimum TMD parameters with a new optimization algorithm, the Archimedes Optimization Algorithm (AOA). They compared AOA with the Jaya Algorithm (JA) and the Modified Jaya Algorithm (SJA), which were applied on the same problem and the results were obtained and AOA outperformed the other algorithms. Aydin et al. (2024b) modified the parameters of the algorithm to optimize the volume of the truss system with AOA. As a result, the effect of the parameters for minimum volume sizing of the truss system was investigated. Coşut et al. (2024) used T-shaped elements for area optimization according to the maximum stress value using Particle Swarm Optimization (PSO). Thus, they concluded with which stress value the minimum area is reached. Aydın et al. (2023d) used the Flower Pollination Algorithm (FPA) to minimize the cost of a reinforced concrete beam. Their analysis of cases with different algorithm parameter values showed that the use of random sp provides the best performance. Aydin et al. (2023) used Archimedes Optimization Algorithm (AOA), Teaching-Learning Based Optimization and Flower Pollination Algorithm to optimize the weight of a cantilever beam. The new algorithm AOA showed effective performance in this problem.

Design optimization stands as a pivotal topic in engineering, particularly in the realm of structural design where minimizing costs holds paramount importance. This study delves into the engineering conundrum of Welded Beam Design, aiming to curtail the beam's cost through the application of machine learning (ML) models, all while adhering to constraints on loading load, shear stress, bending stress, and end deflection. The dataset utilized in this endeavor was meticulously crafted using a metaheuristic optimization algorithm. This hy-

brid algorithm amalgamates the classical Jaya algorithm with the student phase of Teaching Learning Based Optimization (TLBO), furnishing a robust foundation for data generation. Six distinct algorithms were employed for predictive analyses: Linear Regression, Decision Tree, Elastic Net, K-Nearest Neighbour, Random Forest, and the XGBoost algorithm. Due to the presence of multiple outputs in the dataset, Multioutput Regression techniques were employed to ensure accurate modeling and prediction. In this study, both the optimum design of the welded beam has been realised and its optimum design has been predicted by machine learning models.

2. Methodology

2.1. Optimization

Optimization is the process of finding the best values for system parameters among all possible values to optimize the solution to a problem. Since optimization problems exist in every research field, it is necessary to develop optimization techniques (Yang 2010). Optimization aims to find the optimum value among the solutions. Each iteration represents the starting point for the next iteration. When optimization is applied structurally, it aims to find the design that provides cost minimization and the necessary structural requirements. The optimum design includes the most efficient combination of shape, size and topology values. Optimization methods have a certain design framework. Optimization results are required to remain within certain limits. The objective function in optimization is the definition of the value to be kept at minimum level as a function. The aim of optimization is to find the most suitable combination for these variables within the specified limits.

Due to the drawbacks of traditional optimization algorithms, such as being stuck in local optima and the need to specify the search space, interest in metaheuristic optimization approaches has increased in recent decades. When, examining the behaviors of organisms in nature, such as foraging, social behavior, and survival, we find that there are several intelligent approaches. When metaheuristic algorithms inspired by these approaches are created, they yield very good results in solving real-world problems (Fister et al. 2013). Metaheuristic algorithms are used to solve optimization problems and find optimal designs. Depending on the problem type, the objective function is minimized or maximized to produce an optimal design under existing constraints. Metaheuristics are heuristics that are inspired by nature. Metaheuristics aims to use the search space more efficiently by further improving methods. These are often preferred because they can solve large, complex problems. Especially in engineering, solving complex optimization problems is very important. Metaheuristic algorithms can converge to an optimal solution and produce effective solutions in a short time (Osman and Laporte 1996). Metaheuristic optimization algorithms are a type of optimization algorithm designed to solve complex optimization problems that are difficult or impossible to solve using traditional optimization techniques. They work by simulating natural or social processes such as evolution, swarm behaviour (Kennedy and Eberhart 1995) or a process to explore the solution space, finding optimal or near-optimal solutions. The data produced by optimization using metaheuristic algorithms can be used in machine learning. In this study, 1189 data were generated with the Jaya algorithm and used for training in machine learning. In the study, optimization was performed with a hybrid Jaya Algorithm (JA) by using MATLAB2018. The data produced by the optimization were used in machine learning.

2.2. Optimization framework

The Jaya algorithm (JA) outperforms other well-known optimization algorithms in various benchmark problems due to its simplicity and computational efficiency. The Jaya algorithm is a powerful optimization algorithm that shows great promise in solving a wide range of engineering design problems and is a good alternative to more complex and computationally time-consuming optimization techniques. Although JA was developed with a simple logic, it is a very successful algorithm in terms of reaching the optimum solution in a relatively short time.

JA is a single-phase metaheuristic algorithm that uses the worst (g^w) and best (g^*) solutions in a single equation formulation developed by Rao. As Sankrit's name means "victory", by using the best existing solution, the new solution approaches the best solution in the world, but by using the worst solution, we diverge from the worst solution, you can win with optimization (Rao 2016). The Jaya algorithm starts the optimization process with an initial population of randomly selected solutions. The initial solution is randomly generated as Eq. (1).

$$D_{i,j} = \text{rand}(D_1, D_2, \dots, D_n) \quad (1)$$

Next, potential solutions are produced to seek improved alternatives compared to the current solutions, as outlined in Eq. (2). During the candidate solution identification process, the value of each design variable in the relevant solution is adjusted, bringing it nearer to the optimal design within the population and farther from the least favorable design, based on their respective distances (Rao 2016).

$$X_{\text{new}} = X_{\text{old}} + \text{rand}()(g^* - X_{\text{old}}) - \text{rand}()(g^w - X_{\text{old}}) \quad (2)$$

In this formulation, X_{new} and X_{old} are the updated new and existing solutions, respectively. A new solution is generated using a random number between 0 and 1 (rand(0,1)).

Although JA is a single-phase, parameterless algorithm, it is easy to apply, but local optimization can be problematic for JA. Therefore, the second stage is provided by the student stage of TLBO. In this stage of TLBO, two randomly selected existing solutions (X_i and X_j) are used, as shown in Eq. (2). The equation changes depending on the value of the objective function ($f(x)$).

$$X_{\text{new}} = \begin{cases} X_{\text{old}} + \text{rand}()\left(X_i - X_j\right) \text{ if } F(X_i) > F\left(X_j\right) \\ X_{\text{old}} + \text{rand}()\left(X_j - X_i\right) \text{ if } F(X_i) < F(X_j) \end{cases} \quad (3)$$

2.3. Machine learning

Artificial intelligence (AI) is a sub-branch of computer science and has gained a place in academia and industry by enabling computers to behave intelligently. With the development of computer technologies, the desire to give computers the ability to establish relationships between data has led to the emergence of machine learning (ML). Machine learning can train itself with many data and develop new behaviours by using this training for other different conditions. While artificial intelligence is the ability of programs to learn and behave like humans, machine learning is an algorithm written for the same purpose. There are some concepts used for optimization that aim to improve the performance of model prediction. In recent years, researches have been studied in the field of structural design optimization and machine learning applications for predictive modeling (Cakiroglu et al. 2022, 2023a, 2023b; Bekdaş et al. 2023; Cakiroglu and Bekdaş 2023; Liu et al. 2024; Aydin et al. 2024a).

There are many machine learning algorithms based on the learning technique. After the data set is prepared, machine learning algorithms are run to analyse the data. Multiouput regression is performed with these algorithms. The machine learning algorithms are trained using the training data set and then the success of the algorithms is tested on the test data set. The machine learning algorithms used in the study are as follows: Within the scope of the study, 6 different machine learning regression methods including Linear Regression, Decision Tree, Elastic Net, K-Nearest Neighbour, Random Forest and XGBoost algorithms were used for prediction.

2.3.1. Multioutput Regression

Multiple output regression is a machine learning problem in which multiple outputs are predicted based on given inputs. Multiple output regression has a wide range of applications. For example Nguyen et al. (2023) used the multioutput regression to predict the strain and energy absorption capacity of ultra-high performance fibre reinforced concrete (UHPFRC) at the highest tensile stress. Aydın et al. (2023e) applied optimization and multioutput regression together for environmentally friendly reinforced concrete column design.

Increasing the number of outputs to be predicted in machine learning can cause complexity. Because the increase of ML models corresponding to the output may increase the processing lines in the computer. Therefore, in such cases, the Multioutput Regression model (Pedregosa et al. 2011) with accurate predictors selected in the trial and error phase is preferred. In this study, Multioutput Regression will be applied to different ML models and the best model will be determined. Thus, it will be possible to select the right models that can show the best performance in predicting targets using MORM. The dataset in this study has 5 outputs with 3 inputs. Six different predictors including Linear Regression, Decision Tree, Elastic Net, K-Nearest Neighbour, Random Forest and XGBoost algorithms are used. A brief introduction to these models is given in the rest of the paper. Fig. 1 shows the ML process of the study.

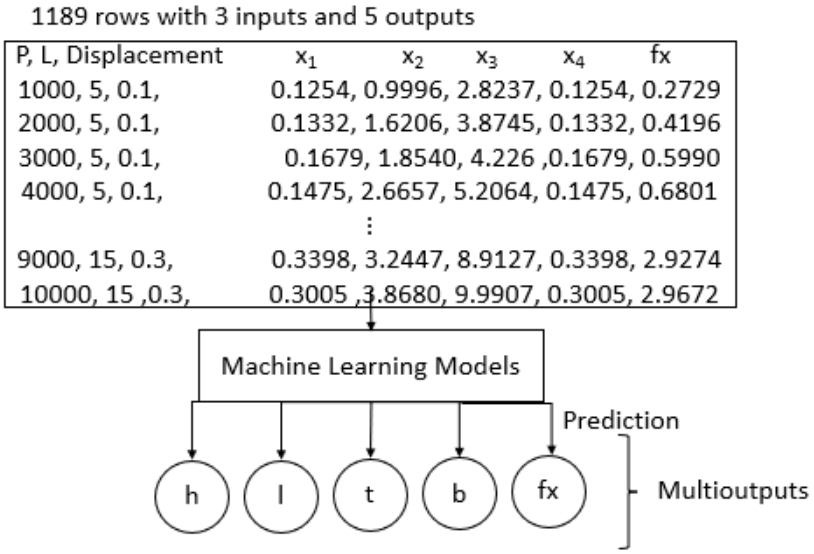

Fig. 1. Machine learning process.

2.3.2. Linear Regression (LR)

Linear regression is a statistical method that assumes a linear relationship between an input variable (x) and a single output variable (y). It seeks to model the relationship between the input and output by fitting a straight line to the observed data points. The linear regression model is characterized by its simplicity and interpretability, making it a popular choice for predicting continuous outcomes when the relationship between variables can be approximated by a straight line.

2.3.3. Decision Tree Regression (DTR)

A decision tree constructs a model for regression or classification represented in a tree-like structure. It iteratively divides the dataset into smaller subsets and builds associated decision trees incrementally. The resulting tree comprises decision nodes and leaf nodes. For soft classification, individual regression trees are constructed for each class. In this approach, the intensity values of pixels across various bands serve as predictor variables or feature vectors, while the known class proportions of the pixels, termed as soft reference data, are the target variables or target vectors for each regression tree. During prediction, intensity values are input into each regression tree, and the model provides estimated class proportions as the output. This process enables the assignment of soft classification probabilities to each class, offering more nuanced insights than traditional binary classification methods (Çene 2022).

2.3.4. ElasticNet Regression (ENT)

Elastic net regression is a variant of linear regression that incorporates a penalty term to adjust predictor coefficients. This penalty term combines both the L1 norm (absolute value) and L2 norm (squared) of the coefficients, weighted by a parameter known as alpha. By leveraging this combination, elastic net regression harnesses the advantages of both Lasso regression and Ridge regression. In essence, elastic net regression is adept at grouping and reducing parameters linked to normalized variables. It provides the flexibility to retain these parameters in the equation or remove them altogether, offering a versatile approach to model selection and feature reduction (Aytekin 2021).

2.3.5. K-Neighbors Regression (KNN)

In the context of regression, KNN is often referred to as "K-nearest neighbor regression" or "KNN regression." It is a simple and intuitive algorithm that makes predictions by finding the K data points closest to a given input and either averaging their target values (in the case of numerical regression) or choosing the majority class. In KNN regression, the distance between the selected observation and other observations is calculated first.

2.3.6. Random Forest Regression (RFR)

The Random Forest (RF) regression algorithm operates as an ensemble learning method, amalgamating a multitude of regression trees. Each regression tree encapsulates a series of conditions or constraints organized hierarchically and applied sequentially from the root to the leaves of the tree. The RF algorithm initiates by generating several bootstrap samples with replacements from the original training dataset. Subsequently, a regression tree is constructed for each bootstrap sample. At each node within every tree, a subset of input variables, randomly selected from the total set, is considered for binary splitting. This randomness injects diversity into the trees, enhancing the robustness and generalization capabilities of the overall ensemble model.

2.3.7. eXtreme Gradient Boosting (XGBoost)

XGBoost stands as a gradient-boosting-based decision tree ensemble meticulously engineered for high scalability. In line with gradient boosting, XGBoost iteratively builds an additive extension of the objective function by minimizing a specified loss function. Notably, XGBoost concentrates solely on decision trees as the fundamental classifier. To regulate the complexity of these trees, a tailored variation of the loss function is employed, ensuring optimal model performance while controlling for overfitting. This meticulous approach allows XGBoost to deliver superior scalability and efficiency in handling diverse datasets and modeling tasks.

2.4. Dataset

To be used in machine learning, a dataset of 1189 rows was obtained using the optimization process. Firstly, by using P, L and displacement values in the optimization performed on MATLAB, a dataset of 1189 rows with optimum size and optimum cost values was obtained. This dataset was used in machine learning. There are 3 inputs and 5 outputs in the data set. Inputs are P, L, and displacement. In the training data, the applied load (P) was taken between 500-10000 lb, length (L) was taken between 5-15 in and the displacement limit was taken as between 0.1-0.3 in. The outputs are h (x_1), l (x_2), t (x_3) and b (x_4) and the objective function, cost. Table 1 shows the statistical properties of the data set.

Table 1. Statistical properties of the data set.

Inputs and outputs	Mean	std deviation	min	max
P (lb)	5478.5534	2878.9704	1000	10000
L (in)	9.9798	3.1677	5.0	15.0
Displacement (in)	0.1997	0.0631	0.1	0.3
x_1 (in)	0.1940	0.0548	0.1250	0.4278
x_2 (in)	2.9981	1.0403	0.9805	5.8534
x_3 (in)	7.0081	1.8172	2.7888	10.0
x_4 (in)	0.1940	0.0548	0.1250	0.4278
f_x	1.3215	0.6628	0.2725	3.0546

From Table 1, the mean value, standard deviation, min and max value of inputs and outputs can be seen. Fig. 2 shows the scatter plot of the dataset. Thus, a comparative scatter between inputs and outputs is shown in each cell. In the diagonal, there are also histograms in which there will be no self-scattering.

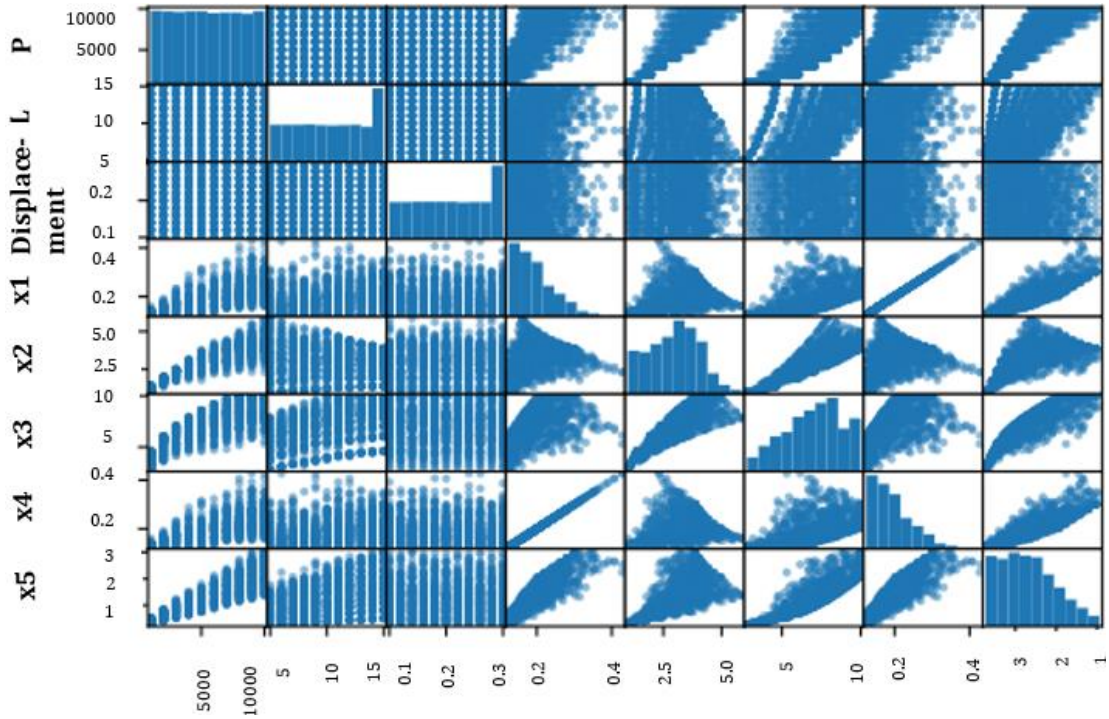

Fig. 2. Scatter plot of dataset.

From Fig. 3, the overall process of the study can be understood. As indicated by Fig. 3, firstly dataset was generated by Jaya Algorithm and achieved best (optimum) results. Then this dataset was used different predictive models and train test split used (30-70%). At the end, the best predictive model is determined.

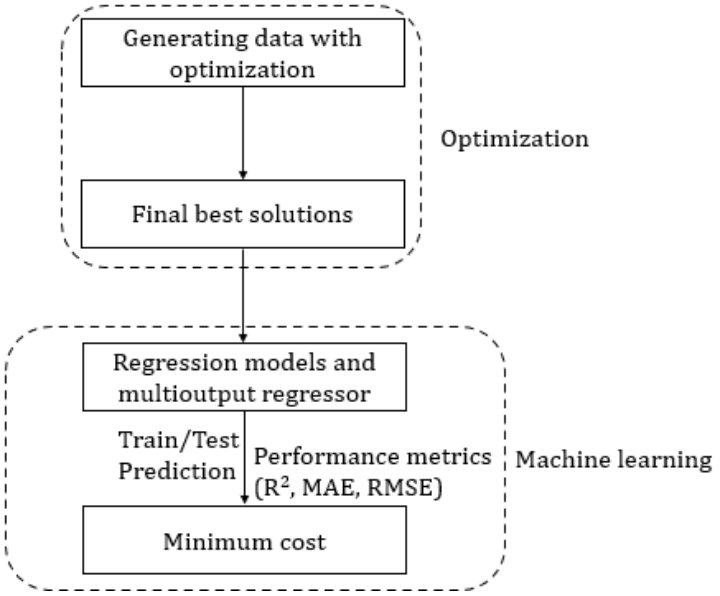

Fig. 3. General framework of the study.

3. The Welded Beam Problem

Welded beams are designed for structural support to withstand buckling under heavy loads. Welded Beams provide a superior durability performance where they are applied. Welded beams are available in a wide range of sizes, do not require preheating for welding, are prefabricated. It has applications in commercial and residential construction, mining and energy facilities, engineering, transport and many other fields. Fig. 4 shows a

rigid member welded to a beam in a welded beam design. As can be seen in the figure, load is applied at the end of the member. The beam will be optimized for minimum cost by varying the weld and member dimensions. The design variables of the problem are shown in Fig. 4 (h (x_1), l (x_2), t (x_3) and b (x_4)).

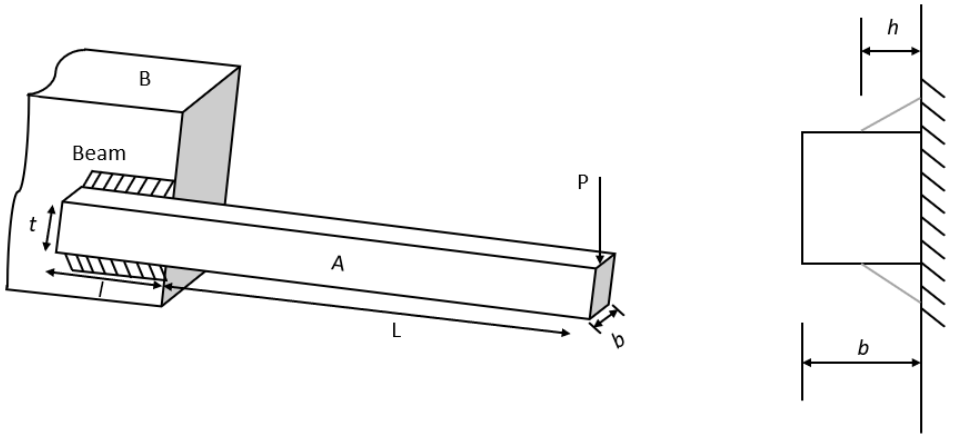

Fig. 4. Welded beam.

The aim of the study, which is to minimize the cost of the cantilever beam design problem, is formulated by Eq. (4).

$$\min(f(x)) = 1.10471{x_1}^2 x_2 + 0.04811 x_3 x_4 (14.0 + x_2) \quad (4)$$

The design constraints consist of shear stress limits (τ), bending stress (σ), buckling load (P_c) and end deflection (δ). The design constraints in the problem are given in Eqs. (5-11) (Savsani 2014).

$$g_1(\mathrm{x}) = \tau(\mathrm{x}) - \tau_{\max} \leq 0 \quad (5)$$

$$g_2(\mathrm{x}) = \sigma(\mathrm{x}) - \sigma_{\max} \leq 0 \quad (6)$$

$$g_3(\mathrm{x}) = x_1 - x_4 \leq 0 \quad (7)$$

$$g_4(\mathrm{x}) = 0.10471{x_1}^2 + 0.048111 x_3 x_4 ((14.0 + x_2) - 5.0 \leq 0 \quad (8)$$

$$g_5(\mathrm{x}) = 0.125 - x_1 \leq 0 \quad (9)$$

$$g_6(\mathrm{x}) = \delta(\mathrm{x}) - \delta_{\max} \leq 0 \quad (10)$$

$$g_7(\mathrm{x}) = \mathrm{P} - P_c \leq 0 \quad (11)$$

The parameters required for the calculation of these constraints are given in Eqs. (12-20).

$$\tau(x) = \sqrt{(\tau')^2 + 2\tau'\tau'' \frac{x_2}{2R} + (\tau'')^2} \quad (12)$$

$$\tau' = \frac{P}{\sqrt{2} x_1 x_2} \quad (13)$$

$$\tau'' = \frac{MR}{J} \quad (14)$$

$$M = P\left(L + \frac{x_2}{2}\right) \quad (15)$$

$$R = \sqrt{\frac{x_2}{4} + \left(\frac{x_1 + x_3}{2}\right)^2} \quad (16)$$

$$J = 2\left[\sqrt{2} x_1 x_2 \left\{\frac{x_2^2}{12} + \left(\frac{x_1 + x_3}{2}\right)^2\right\}\right] \quad (17)$$

$$\sigma(x) = \frac{6PL}{x_4 x_3^2} \quad (18)$$

$$\delta(x) = \frac{6PL^3}{E x_4 x_3^3} \quad (19)$$

$$P_c(x) = \frac{4.013E\sqrt{\frac{x_3^2 x_4^6}{36}}}{L^2}\left(1 - \frac{x_3}{2L}\sqrt{\frac{E}{4G}}\right) \quad (20)$$

Here E=30·10^6 psi, G = 12·10^6 psi, $\tau_{\max}$= 13600 psi, $\sigma_{\max}$=30000 psi. With the first constraint (g_1), it is ensured that the maximum shear stress developed is less than the safe shear stress of the weld material. With the second constraint (g_2), it is checked whether the maximum normal stress developed is less than the safe normal stress in the beam. The third to fifth constraints (g_3 - g_5) ensure that the geometric dimensions are suitable for design. The sixth constraint (g_6) ensures the displacement limit of the beam. The seventh constraint (g_7) ensures that the load on the beam is not greater than the safe buckling load. In the equations, M is the moment, P is the force on the beam and P_c is the buckling load on the bar (Akyol and Feneaker 2022).

4. Results and Discussion

The performance of regression models was assessed using key metrics such as the Coefficient of Determination (R^2), Mean Absolute Error (MAE), and Root Mean Square Error (RMSE). R^2 quantifies the proportion of variability in the dependent variable explained by the model. MAE represents the average magnitude of prediction errors, while RMSE provides a measure of the typical magnitude of these errors. While individual results

may not offer substantial insights, they serve as numerical benchmarks for comparing different model performances, aiding in the selection of the most suitable regression model. RMSE is derived from the square root of MSE, where MSE quantifies the average squared difference between predicted and actual values. MAE, on the other hand, calculates the average of all absolute prediction errors. Performance metrics for the machine learning models employed in this study are presented in Table 2.

Table 2. Performance metrics of ML models.

Model	R^2	MAE	RMSE
Linear Regression	0.7550	0.2318	0.2886
Decision Tree Regressor	1.0	6.1344e-11	9.4637e-10
Elastic Net Regressor	0.6951	0.2432	0.3089
K Neighbors Regressor	0.8359	0.1343	0.1999
Random Forest Regressor	0.9647	0.0604	0.0935
XGBoost	0.9660	0.0611	0.0860

According to the results in the Table 2, the R^2 value of the Decision Tree is 1. This value was obtained as 0.7550, 0.6951, 0.8359, 0.9647 and 0.9660 with Linear Regression, ElasticNet, KNN, RFR and XGBoost algorithms respectively. As a result of the analysis, DTR showed both the fastest and the most successful performance for minimum cost prediction. Decision Tree was the most successful ML model in predicting the values to minimize the cost. It has the highest R^2 and the lowest error values. It is followed by XGBoost, which is very close to Random Forest. Linear Regression performed the worst with the lowest R^2 and the highest error values.

5. Conclusions

In structural design, economy is an indispensable element as long as it does not harm reliability. Nowadays, very large amounts of data can be accessed using optimization. With the ability to generate data using optimization and the development of machine learning methods that can process the data, it is possible to reduce costs in structural engineering design. The main objective of this study is to apply machine learning algorithms to engineering design and to realize less costly design. For this purpose, load, length and displacement were determined as input and b, h, l, t, minimum cost were determined as output. By using these input and output data, Linear Regression, Decision Tree, Elastic Net, K-Nearest Neighbour, Random Forest, and XGBoost algorithms, the result that will give the minimum cost of the welded beam is reached.

In this research, optimization and machine learning are performed together. The performance of ML models were compared using Python. Based on the comparison of these results, Decision Tree Regression was superior (R^2=1, MAE=6.13e-11, RMSE=9.47e-10) to other ML models for the prediction of minimum cost design. In summary, this study demonstrates that optimization and ML models could be used effectively to design with minimum cost.

Acknowledgements
None declared.

Funding
The authors received no financial support for the research, authorship, and/or publication of this manuscript.

Conflict of Interest
The authors declared no potential conflicts of interest with respect to the research, authorship, and/or publication of this manuscript.

Author Contributions
All of the authors made substantial contributions to conception and design, or acquisition of data, or analysis and interpretation of data; were involved in drafting the manuscript or revising it critically for important intellectual content; and gave final approval of the version to be published.

Data Availability
The datasets created and/or analyzed during the current study are not publicly available, but are available from the corresponding author upon reasonable request.

References

Akyol K, Feneaker SOF (2022). Chaotic multi-swarm particle swarm optimization for welded beam design engineering problem. *Politeknik Journal*, 25(4), 1645-1660.

Arslan H, Fatih Ü, Demirci M, Taşar B, Yılmaz A (2020). Estimation of Keban Dam Lake level change using ANFIS and support vector machines. *Osmaniye Korkut Ata University Journal of Institute of Science and Technology*, 3(2), 71-77.

Aydın Y, Bekdaş G, Nigdeli SM, Isıkdağ Ü, Kim S, Geem ZW (2023a). Machine learning models for ecofriendly optimum design of reinforced concrete columns. *Applied Sciences*, 13(7), 4117.

Aydın Y, Işıkdağ Ü, Bekdaş G, Nigdeli SM, Geem ZW (2023b). Use of machine learning techniques in soil classification. *Sustainability*, 15(3), 1-18.

Aydın Y, Cakiroglu C, Bekdaş G, Işıkdağ Ü, Kim S, Hong J, Geem ZW (2023c). Neural network predictive models for alkali-activated concrete carbon emission using metaheuristic optimization algorithms. *Sustainability*, 16(1), 1-20.

Aydın Y, Bekdaş G, Nigdeli SM (2023d). Reinforced concrete beam optimization via flower pollination algorithm by changing switch probability parameter. *In: Vasan, P, et al. editors. Intelligent Computing and Optimization. ICO 2023. Lecture Notes in Networks and Systems*, vol 852. Springer, Cham. 66-74.

Aydin Y, Nigdeli SM, Bekdaş G (2023e). Archimedes Optimization Algorithm on a Structural Optimization Problem. *In: Vasant P, et al. editors. Intelligent Computing and Optimization (ICO 2023). Lecture Notes in Networks and Systems,* vol 854. Springer, Cham. 173-180.

Aydin Y, Nigdeli SM, Bekdaş G (2024a). Archimedes optimization algorithm for optimization of tuned mass dampers in structural control. *SSRN* (https://ssrn.com/abstract=4750319), 1-8.

Aydin Y, Nigdeli SM, Bekdaş G (2024b). Parametric investigation of archimedes optimization algorithm for a structural problem. *SSRN* (https://ssrn.com/abstract=4750288), 1-8.

Aytekin HT (2021). The potential importance of machine learning in the context of researchers data analysis. *Ufuk University Social Sciences Institute Journal*, 10(19), 85-106.

Bekdaş G, Nigdeli SM (2011). Estimating optimum parameters of tuned mass dampers using harmony search. *Engineering Structures*, 33(9), 2716-2723.

Bekdaş G, Nigdeli SM (2013). Mass ratio factor for optimum tuned mass damper strategies. *International Journal of Mechanical Sciences*, 71, 68-84.

Bekdaş G (2015). Harmony search algorithm approach for optimum design of post-tensioned axially symmetric cylindrical reinforced concrete walls. *Journal of Optimization Theory and Applications*, 164, 342–358.

Bekdaş G, Nigdeli SM, Yang XS (2015). Sizing optimization of truss structures using flower pollination algorithm. *Applied Soft Computing*, 37, 322-331.

Bekdaş G, Nigdeli SM (2016). Bat algorithm for optimization of reinforced concrete columns. *PAMM*, 16(1), 681-682.

Bekdaş G, Cakiroglu C, Islam K, Kim S, Geem ZW (2022). Optimum design of cylindrical walls using ensemble learning methods. *Applied Sciences*, 12(4), 2165. 1-16.

Bekdaş G, Cakiroglu C, Kim S, Geem ZW (2022). Optimization and predictive modeling of reinforced concrete circular columns. *Materials*, 15(19), 6624, 1-18.

Bekdaş G, Aydın Y, Isıkdağ Ü, Sadeghifam AN, Kim S, Geem ZW (2023). Prediction of cooling load of tropical buildings with machine learning. *Sustainability*, 15(11), 9061. 1-20.

Bekdaş G, Cakiroglu C, Kim S, Geem ZW (2023). Optimal dimensions of post-tensioned concrete cylindrical walls using harmony search and ensemble learning with SHAP. *Sustainability*, 15(10), 7890, 1-18.

Cakiroglu C, Islam K, Bekdaş G, Billah M (2021). CO2 emission and cost optimization of concrete-filled steel tubular (CFST) columns using metaheuristic algorithms. *Sustainability*, 13(14), 8092, 1-16.

Cakiroglu C, Islam K, Bekdaş G, Isikdag U, Mangalathu S (2022). Explainable machine learning models for predicting the axial compression capacity of concrete filled steel tubular columns. *Construction and Building Materials*, 356, 129227, 1-20.

Cakiroglu C, Bekdaş G (2023). Predictive modeling of recycled aggregate concrete beam shear strength using explainable ensemble learning methods. *Sustainability*, 15(6), 4957, 1-16.

Cakiroglu C, Islam K, Bekdaş G (2023a). Manta ray foraging and jaya hybrid optimization of concrete filled steel tubular stub columns based on CO_2 emission. *In: Bekdaş G, Nigdeli SM (eds) Hybrid Metaheuristics in Structural Engineering. Studies in Systems, Decision and Control*, vol 480. Springer, Cham. 111-125.

Cakiroglu C, Islam K, Bekdaş G, Nehdi ML (2023b). Data-driven ensemble learning approach for optimal design of cantilever soldier pile retaining walls. *Structures*, 51, 1268-1280.

Cao Y, Wakil K, Alyousef R, Jermsittiparsert K, Ho LS, Alabduljabbar H, Mohamed AM (2020). Application of extreme learning machine in behavior of beam to column connections. *Structures*, 25, 861-867.

Çoşut M, Bekdaş G, Nigdeli SM (2024). Area optimization for a T-shaped element by using pure bending equation and particle swarm optimization. *SSRN* (https://ssrn.com/abstract=475182), 1-8.

Çene E (2022). Predicting Euroleague basketball match outcomes with machine learning techniques and revealing the most important game related variables. *Journal of Sports and Performance Research*, 13(1), 31-54.

Dogan G, Arslan MH, Baykan OK (2020). Determination of damage levels of RC columns with a smart system oriented method. *Bulletin of Earthquake Engineering*, 18(7), 3223-3245.

Fister Jr I, Yang XS, Fister I, Brest J, Fister D (2013). A brief review of nature-inspired algorithms for optimization. *Elektrotehniški vestnik, Journal of Electrical Engineering and Computer Science*, 80(3), 1-7.

Huang Q, Cox RF, Shaurette M, Wang J (2012). Intelligent building hazard detection using wireless sensor network and machine learning techniques. *In: Raymond Issa R, Flood I, editors. Computing in Civil Engineering*, ASCE Reston VA, USA. 485-492.

Jeon JS, Shafieezadeh A, DesRoches R (2014). Statistical models for shear strength of RC beam-column joints using machine-learning techniques. *Earthquake Engineering & Structural Dynamics*, 43(14), 2075-2095.

Kayabekir AE, Sayın B, Nigdeli SM, Bekdaş G (2018). Jaya algorithm based optimum carbon fiber reinforced polymer design for reinforced concrete beams. *AIP Conference Proceedings,* 1978(1), 1-4.

Liu T, Cakiroglu C, Islam K, Wang Z, Nehdi ML (2024). Explainable machine learning model for predicting punching shear strength of FRC flat slabs. *Engineering Structures*, 301, 117276, 1-20.

Nguyen NH, Abellán-García J, Lee S, Nguyen TK, Vo TP (2023). Simultaneous prediction the strain and energy absorption capacity of ultra-high performance fiber reinforced concretes by using multi-output regression model. *Construction and Building Materials*, 384, 131418. 1-20.

Okazaki Y, Okazaki S, Asamoto S, Chun PJ (2020). Applicability of machine learning to a crack model in concrete bridges. *Computer-Aided Civil and Infrastructure Engineering*, 35(8), 775-792.

Osman IH, Laporte G (1996). Metaheuristics: A bibliography. *Annals of Operations Research*, 63, 513-623.

Pedregosa F, Varoquaux G, Gramfort A, Michel V, Thirion B, Grisel O, Duchesnay É (2011). Scikit-learn: Machine learning in Python. *The Journal of Machine Learning Research*, 12, 2825-2830.

Rao R (2016). Jaya: A simple and new optimization algorithm for solving constrained and unconstrained optimization problems. *International Journal of Industrial Engineering Computations*, 7(1), 19-34.

Savsani V (2014). Implementation of modified artificial bee colony (ABC) optimization technique for minimum cost design of welded structures. *International Journal for Simulation and Multidisciplinary Design Optimization*, 5, 1-16.

Steel Force. Welded Beams. https://www.steelforce.com.au [accessed 20-03-2024].

Ulusoy S, Niğdeli SM, Bekdaş G (2019). Optimization of PID controller parameters for active control of single degree of freedom structures. *Challenge Journal of Structural Mechanics*, 5(4), 130-140.

Ulusoy S, Kayabekir AE, Bekdaş G, Nigdeli SM (2020). Metaheuristic algorithms in optimum design of reinforced concrete beam by investigating strength of concrete. *Challenge Journal of Concrete Research Letters*, 11(2)- 26-30.

Yang XS (2010). Nature-Inspired Metaheuristic Algorithms. Luniver Press, UK.

Yücel M, Nigdeli SM, Kayabekir AE, Bekdaş G (2021). Optimization and artificial neural network models for reinforced concrete members. *In: Carbas S, Toktas A, Ustun D, editors. Nature-Inspired Metaheuristic Algorithms for Engineering Optimization Applications*. Springer Tracts in Nature-Inspired Computing. Springer, Singapore. 181-199.

Yücel M, Bekdaş G, Nigdeli SM, Kayabekir AE (2021). An artificial intelligence-based prediction model for optimum design variables of reinforced concrete retaining walls. *International Journal of Geomechanics*, 21(12), 04021244, 1-20.

Challenge Journal of Structural Mechanics

Research Article

The effect of build direction on component strength in SLA-based additive manufacturing

Hojjat Ghahramanzadeh Asl [a,*], Derya Karaman [a]

[a] *Department of Mechanical Engineering, Karadeniz Technical University, 61080 Trabzon, Türkiye*

ABSTRACT

Nowadays additive manufacturing is frequently used, especially in industrial applications such as aerospace and biomedical. In the additive manufacturing method, thanks to the layered manufacturing technique, it enables the production of components with all kinds of complex geometries and accelerates the production process. As it is known, the orientation of the layers in the additive manufacturing technique affects the mechanical properties of the components. Among the parameters affecting strength, layer thickness, production direction and layer geometry are of great importance. In this study, the effect of layer orientation on component strength in SLA-based additive manufacturing was experimentally investigated. Consequently, standard tensile samples were produced at four different production orientation using the UV Stereolithography method. Tests of the tensile samples were carried out at constant tensile speed and tensile curves were obtained. According to the results, it was determined that the layer joints parallel to the shear plane exhibited the lowest strength. Therefore, samples produced at the parallel to the shear plane fractures at lower loads and showed low strength. Considering the experimental results obtained, it has been determined that the structure orientation affects the mechanical properties of the component by ~20%.

ARTICLE INFO

Article history:
Received 11 April 2024
Revised 20 May 2024
Accepted 3 June 2024

Keywords:
SLA-based additive manufacturing
Build orientation
Tensile testing
Mechanical properties

1. Introduction

Additive manufacturing is a production process in which the material is added layer by layer using sliced three-dimensional data. It is utilized in various fields such as the automotive industry, defense sector, biomedical field, and consumer sector, helping to overcome limitations often encountered in traditional production techniques (Chong et al. 2018; Mohanavel et al. 2021; Wang et al. 2021). Additive manufacturing technology is highly popular, particularly in the production of parts with complex geometries.

There are many 3D printing technologies available to better respond to industry applications. Among these, fused deposition modelling (FDM), stereolithography (SLA), selective laser sintering (SLS) technologies have been developed by commercial companies and are widely used today (Sürmen et al. 2019). In addition to obtaining the desired geometric properties of the parts with the additive manufacturing technology, the mechanical performance in the field of use is also very important (Tymrak et al. 2014; Chacón et al. 2017). Many parameters such as continuity in layer geometries, layer thickness, layer adhesion performance, position of layers according to part load balance, production surface quality affect the mechanical effect of these parts (Sheoran et al. 2020). Wang et al. performed experimental and numerical analyzes to determine the effects of layer thickness and printing angle for the elastoplastic structure. Based on the data acquired from the study, it was observed that the elastic modulus and tensile strength decrease as the layer thickness increases (Wang et al. 2020). Matos et al. proposed multi-objective approximation functions to assist in determining the optimal build orientation for part production. These objective functions were developed based on parameters such

* *Corresponding author*. Tel.: +90-462-377-3149 ; E-mail address: h.kahramanzade@ktu.edu.tr (H. Ghahramanzadeh Asl)
ISSN: 2149-8024 / DOI: https://doi.org/10.20528/cjsmec.2024.03.002

as the requirement for support structures, production time, surface roughness, and overall surface quality (Matos et al. 2021). Shim et al. (2020) examined the effect of printing orientation in additive manufacturing on surface characteristics and microbial adhesion, as well as mechanical properties. They have experimentally proven that they get the best results from the researched findings with 0 degree production orientation according to positioning. Hada et al. (2020) produced the maxillary prosthesis models with different angles (0°, 45°, and 90°) to assess the impact of production direction on the accuracy of model. They found that the printing direction set at 45° yielded the highest production accuracy. Al‐Dulaijan et al. (2023) experimentally confirmed that for production orientations grouped as 0.45 and 90 degrees, the highest bending strength values were obtained from production parts with 0 degrees. In addition, they stated that high energy was required for crack propagation and that these properties increased significantly as the curing time increased. Li and Teng (2024), emphasized that tensile strength is affected by printing orientation, explained that the strength decreases with increasing orientation angle with a linear correlation.

Additive manufacturing is very often preferred for the production of complex geometries with its development in the design configuration in the field. Complex geometries have internal structures with angle values that differ according to the direction of manufacturing. The aim of this study is to experimentally investigate the changes in the mechanical differences that the build orientation will create in the structure. Standard tensile samples are produced with SLA method at different build orientations (0°, 30°, 45°, and 90°) and subjected to mechanical tests. A stress-strain curve is generated for each individual sample.

2. Materials and Method

Standard tensile samples were taken as reference in the study. Tensile samples were modeled in accordance with ASTM D638 (Fig. 1).

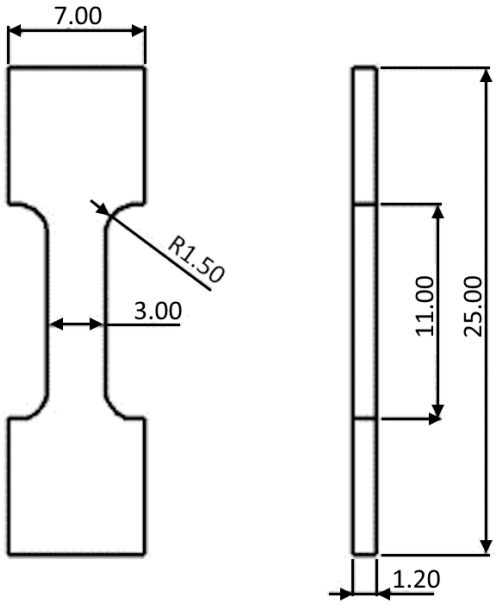

Fig. 1. The tensile test samples dimensions.

Tensile samples were positioned on the build platform at 0°, 30°, 45°, and 90° angle values according to the build direction (Fig. 2). Fig. 2 was showed the visualization that the layers will have the same layer spacing and different layer numbers according to the placements at different angles.

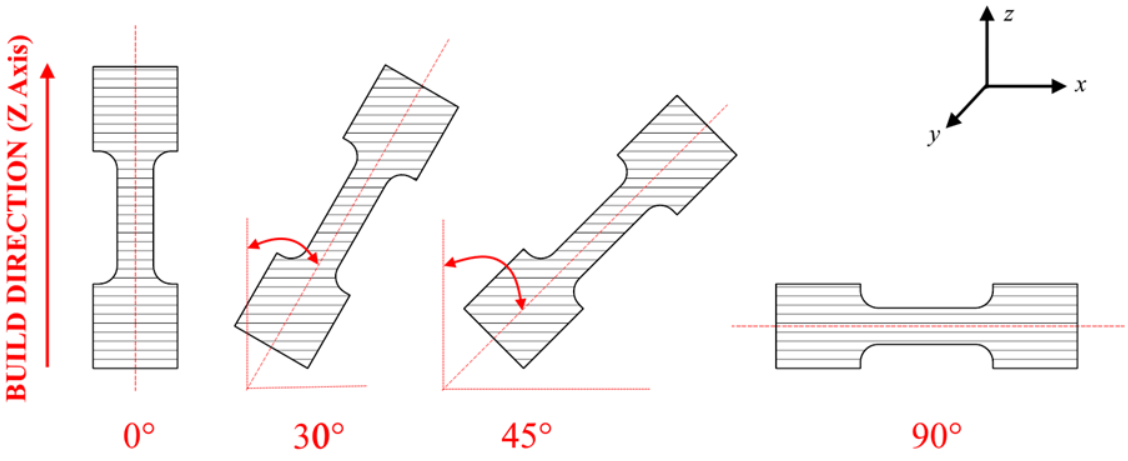

Fig. 2. The build orientation of tensile samples production.

Stereolithography (SLA) technology, one of the additive manufacturing methods, was preferred for production (Fig. 3). With this technology, the build platform is immersed in the liquid resin tank for each production layer, and solidification is carried out with the ultraviolet rays. It provides solidification of parts in desired geometries in a short time with ultraviolet rays.

The production device used was the Anycubic Photon M3 3D printer model (Fig. 4a). A gray liquid resin from the SLA printer's brand was utilized. Five samples were generated for each build orientation. The layer thickness was set to 0.05 mm and the normal exposure time was set to 2 s. After the production period of approximately 1 hour and 45 minutes, the samples were washed with ethanol alcohol together with the build platform (Fig. 4b). Afterwards, the samples were separated from the build platform and placed in the curing device of the same brand for curing. The curing process was carried out in 10 minutes (Fig. 4c).

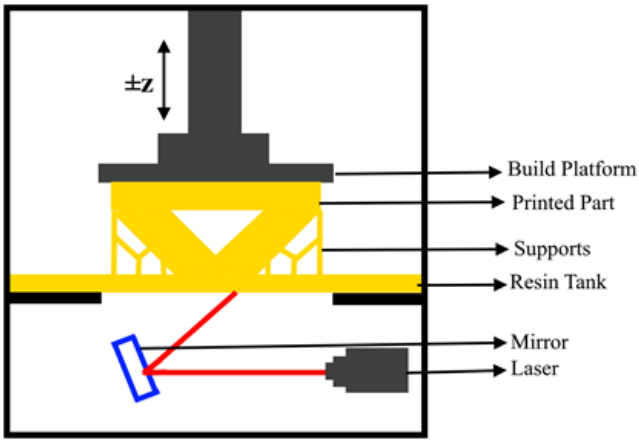

Fig. 3. UV Stereolithography method, one of the additive manufacturing technologies.

The mechanical performances of the samples were evaluated by tensile tests. Tensile tests were performed using the INSTRON 3382 brand (Fig. 5). Three samples at each angle value were tested. Strain at a rate of 0.5 mm/min was applied until fracture was observed in the samples. Metal plates were attached to both grip section of the samples. This prevented the compression of the polyethylene materials in the tensile samples between the grips of the tensile machine.

3. Results and Discussion

Tensile samples produced using SLA were visualized using light microscopy (Fig. 6). The layer orientation of samples with different build orientations was described. The enlarged layer lines depicted in Fig. 1 were obtained in consistent directions during production. The green lines indicated the layer direction, serving as indicators of the desired build orientations.

Three tensile tests were performed for each orientation. Data for each angle was created by taking the average of repeated tests. As a result of the tensile tests, the stress-strain curves of the samples in different build orientations were added as Fig. 7. Tensile samples had a typical curve like ductile materials.

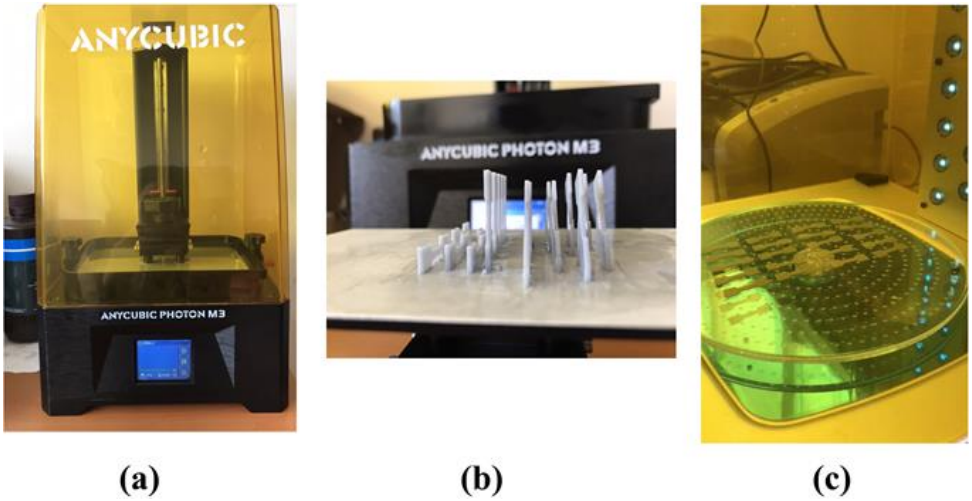

Fig. 4. (a) Anycubic Photon M3 model printer used for production; (b) Post-production sample images; (c) The curing process applied to the samples.

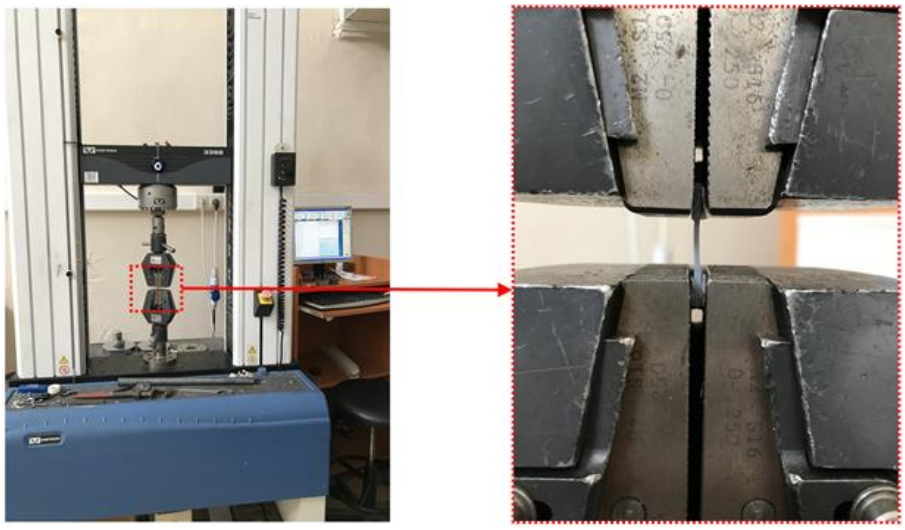

Fig. 5. The tensile testing machine and the specimens being tested.

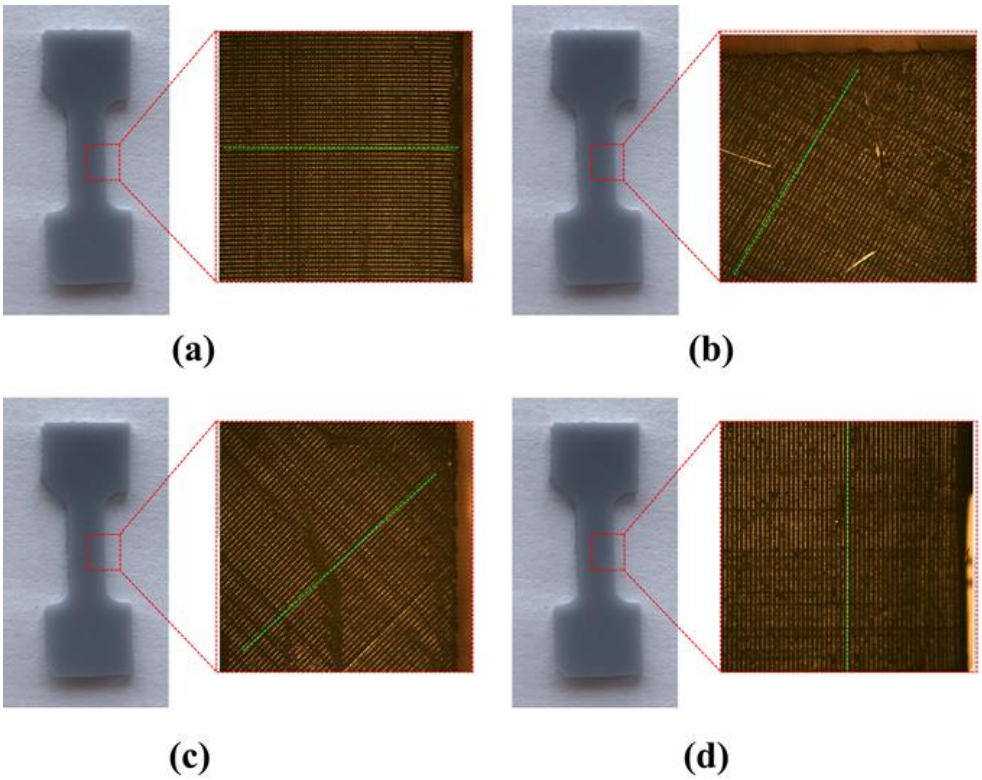

Fig. 6. Post-production images: (a) 0°; (b) 30°; (c) 45°; and (d) 90° samples.

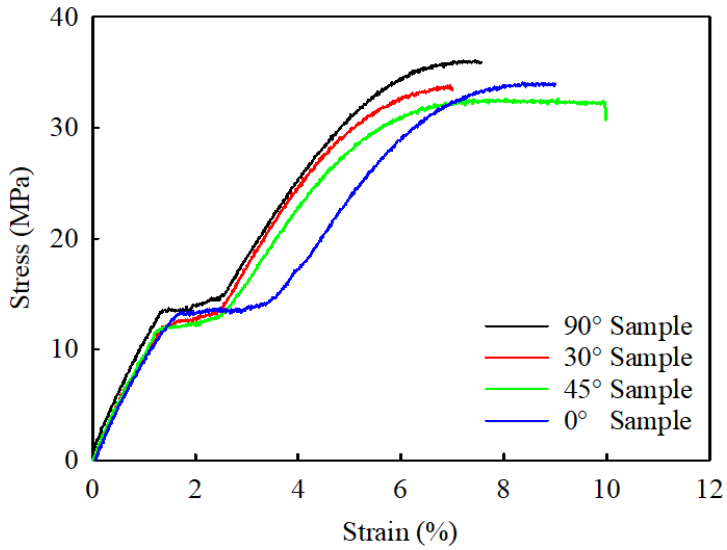

Fig. 7. Stress–strain curve: (a) 0°; (b) 30°; (c) 45°; and (d) 90° samples.

The samples with the same cross-sectional area fractured at different strain and stress values relative to each other. While 90° samples had the highest ultimate strength, 45° samples had the lowest. However, the 45° samples had the highest strain rate. The experimental results of the samples were added to Table 1.

Table 1. Average tensile test data and standard deviation for each manufacturing orientation.

Sample	Yield strength (MPa)	Strain (%)	Ultimate strength (MPa)
0°	13.1805 ± 0.46	9.0103 ± 1.17	33.9613 ± 2.13
30°	11.1325 ± 0.98	6.9934 ± 0.49	33.3697 ± 1.5
45°	12.0127 ± 0.99	9.9815 ± 0.41	33.44993 ± 1.31
90°	13.0798 ± 1.6	7.5654 ± 0.27	35.9398 ± 4.36

According to the yield strength in Table 1, the 30° samples had the lowest strength. 0° showed the highest yield strength. When the yield strength is listed quantitatively, the yield strength increases respectively: 30°, 45°, 90°, and 0°. There is approximately a 1% difference between the yield strength of 0° and 90° samples.

The strain rate value increases between 30°, 90°, 0° and 45° samples, respectively. Ultimate strength was also a precursor to the mechanical difference in build orientation. Also, the 45° sample with the highest strain value had the lowest ultimate strength. The 90° sample had the highest ultimate strength. Fracture images of tensile samples with different build orientations were in Fig. 8.

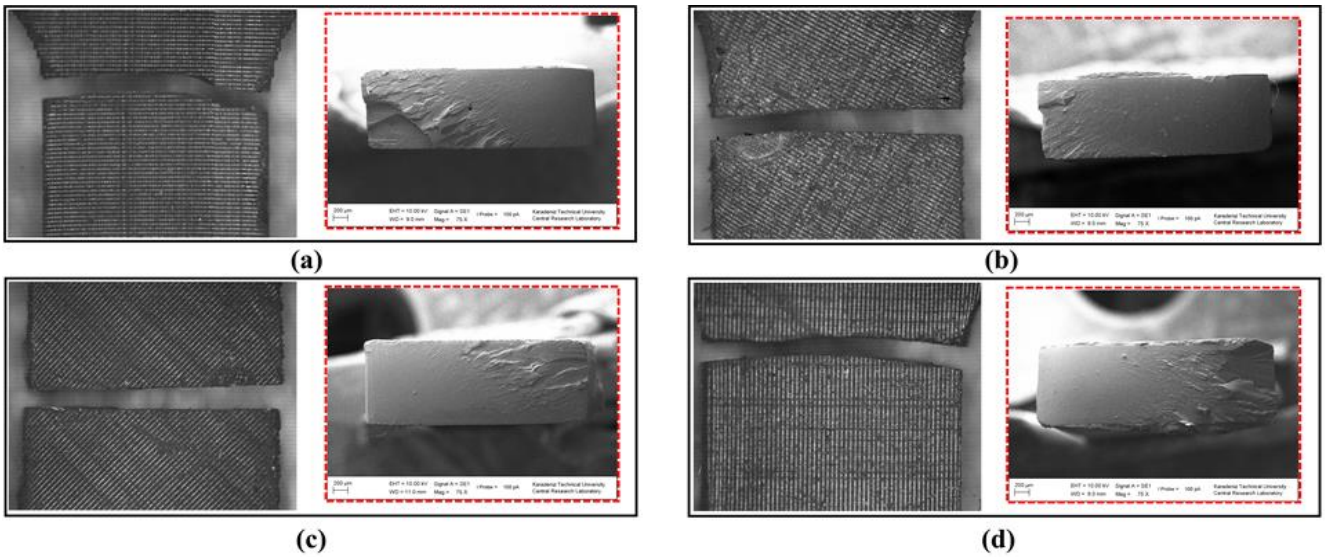

Fig. 8. The fractures samples surface after tensile test: (a) 0°; (b) 30°; (c) 45°; (d) 90°.

The fracture mechanism in the 0° samples was shear failure type (Fig. 7a) (Pelleg et al. 2021). This fracture, which is considered to be very ductile, originates from the layer merge planes. The plastic behavior in the interlayer adhesion regions produced parallel to the x-plane is higher than the layer structure (Aliheidari et al. 2018). The difference in ductile behavior caused the fractures to occur in the fracture plane close to 45°. In 30° samples, the fracture plane was perpendicular to the loading direction (Fig. 7b). This fracture mechanism type shows that the structure exhibits less ductile behavior. The fact that it had the lowest strain rate (Table 1) was proof of that. The fracture plane of the 45° samples was also parallel to the x plane, but the strain rate of the structure was the highest compared to the other structures (Fig. 7c). As it is known, the maximum shear stress in structures occurs at 45° (Goh et al. 2021). Maximum shear stresses occurring in tensile specimens with 45° build orientation are in the same plane with the layer merges. Farkas et al. (2023) noted in their experimental study that the fracture plane was "V" shaped. They stated the reason for this is the eccentric tensile load according to the layer combinations. It is also encountered in these samples that the plastic behavior between the layers is more than the layer. This is proof that it has the highest ductility despite the lowest ultimate strength. A fully ductile fracture type was observed as the fracture mechanism in the 90° specimens (Fig. 6d). However, the data in Table 1 indicate that the ductile behavior of the structure is lower compared to the 0° and 45° samples. The main reason for the occurrence of this type of fracture is the ductile behavior difference between the layer interior structure and the interlayer points (Aliheidari et al. 2018). Layers that are less ductile have higher tensile strength but lower deformation. The tensile strength of the layer junction planes after a layer has broken is low, but the ductility is partially higher.

It was evident from the experimental results that the build orientation affected the mechanical properties of the tensile specimens. The same situation is observed in samples produced with different additive manufacturing technologies (Wang et al. 2021; Patadiya et al. 2018). In various studies, it has been experimentally stated that production accuracy, surface roughness and especially mechanical properties vary depending on the angle of the layers with the production platform (Naik and Kiran 2018; Coppola et al. 2022). This will assist in evaluating the mechanical properties of porous structures popular with additive manufacturing technology (Günther et al. 2022), considering especially its lightness superiority (Ghahramanzadeh Asl and Karaman 2024). Complex geometry surfaces of porous structures have different angles with respect to the production plane. Different effects can be observed on the surfaces as a result of mechanical loading in the porous structures produced. This situation may be related to build orientation and this effect is proven once again by this study.

4. Conclusions

In this study, the effects of build orientation on the mechanical performance of structures in additive manufacturing technologies were investigated. Tensile specimens with 0°, 30°, 45°, and 90° build orientations were produced with SLA. Stress-strain curves of the samples

were obtained by tensile tests performed with a constant strain rate. In terms of ultimate strength, 90° samples had the highest ultimate strength, while 45° samples had the lowest ultimate strength. 30° samples had higher ultimate strength than 0° and 45° samples. However, rupture occurred at the lowest strain rate of the four samples. It has been proved by the experimental results that the build orientation is directly effective in structural mechanics.

Acknowledgements

None declared.

Funding

The authors received no financial support for the research, authorship, and/or publication of this manuscript.

Conflict of Interest

The authors declared no potential conflicts of interest with respect to the research, authorship, and/or publication of this manuscript.

Author Contributions

All of the authors made substantial contributions to conception and design, or acquisition of data, or analysis and interpretation of data; were involved in drafting the manuscript or revising it critically for important intellectual content; and gave final approval of the version to be published.

Data Availability

The datasets created and/or analyzed during the current study are not publicly available, but are available from the corresponding author upon reasonable request.

REFERENCES

AlDulaijan YA, Alsulaimi L, Alotaibi R, Alboainain A, Akhtar S, Khan SQ, Gad MM (2023). Effect of printing orientation and postcuring time on the flexural strength of 3D-printed resins. *Journal of Prosthodontics,* 32(S1), 45-52.

Aliheidari N, Christ J, Tripuraneni R, Nadimpalli S, Ameli A (2018). Interlayer adhesion and fracture resistance of polymers printed through melt extrusion additive manufacturing process. *Materials & Design*, 156, 351-361.

Chacón JM, Caminero MA, García-Plaza E, Núnez PJ (2017). Additive manufacturing of PLA structures using fused deposition modelling: Effect of process parameters on mechanical properties and their optimal selection. *Materials & Design*, 124, 143-157.

Chong L, Ramakrishna S, Singh S (2018). A review of digital manufacturing-based hybrid additive manufacturing processes. *The International Journal of Advanced Manufacturing Technology*, 95, 2281-2300.

Coppola B, Schmitt J, Lacondemine T, Tardivat C, Montanaro L, Palmero P (2022). Digital light processing stereolithography of zirconia ceramics: Slurry elaboration and orientation-reliant mechanical properties. *Journal of the European Ceramic Society*, 42(6), 2974-2982.

Farkas AZ, Galatanu SV, Nagib R (2023). The influence of printing layer thickness and orientation on the mechanical properties of DLP 3D-printed dental resin. *Polymers*, 15(5), 1113.

Ghahramanzadeh Asl H, Karaman D (2024). The novelty design method in lightweight structures with low effective elastic modulus. *Challenge Journal of Structural Mechanics*, 10(2), 47-57.

Goh GD, Toh W, Yap YL, Ng TY, Yeong WY (2021). Additively manufactured continuous carbon fiber-reinforced thermoplastic for topology optimized unmanned aerial vehicle structures. *Composites Part B: Engineering*, 216, 108840.

Günther F, Hirsch F, Pilz S, Wagner M, Gebert A, Kästner M, Zimmermann M (2022). Structure-property relationships of imperfect additively manufactured lattices based on triply periodic minimal surfaces. *Materials & Design*, 222, 111036.

Hada T, Suzuki T, Minakuchi S, Takahashi H (2020). Reduction in maxillary complete denture deformation using framework material made by computer-aided design and manufacturing systems. *Journal of the Mechanical Behavior of Biomedical Materials,* 103, 103514.

Li Y, Teng Z (2024). Effect of printing orientation on mechanical properties of SLA 3D-printed photopolymer. *Fatigue & Fracture of Engineering Materials & Structures*, 47(5), 1531-1545.

Matos MA, Rocha AMA, Costa LA (2021). Many-objective optimization of build part orientation in additive manufacturing. *The International Journal of Advanced Manufacturing Technology*, 112, 747-762.

Mohanavel V, Ali KA, Ranganathan K, Jeffrey JA, Ravikumar MM, Rajkumar S (2021). The roles and applications of additive manufacturing in the aerospace and automobile sector. *Materials Today: Proceedings*, 47, 405-409.

Naik DL, Kiran R (2018). On anisotropy, strain rate and size effects in vat photopolymerization based specimens. *Additive Manufacturing*, 23, 181-196.

Patadiya N H, Dave H K, Rajpurohit S R (2020). Effect of build orientation on mechanical strength of FDM Printed PLA. *Advances in Additive Manufacturing and Joining: Proceedings of AIMTDR 2018 Springer Singapore,* 301-307.

Pelleg J (2021). Fracture in nano-structures. *In: Mechanical Properties of Nanomaterials: Engineering Materials*. Springer, Cham.

Sheoran AJ, Kumar H (2020). Fused deposition modeling process parameters optimization and effect on mechanical properties and part quality: Review and reflection on present research. *Materials Today: Proceedings*, 21, 1659-1672.

Shim JS, Kim JE, Jeong SH, Choi YJ, Ryu JJ (2020). Printing accuracy, mechanical properties, surface characteristics, and microbial adhesion of 3D-printed resins with various printing orientations. *The Journal of Prosthetic Dentistry*, 124(4), 468-475.

Sürmen HK (2019). Eklemeli İmalat (3B Baskı): Teknolojiler ve Uygulamalar. *Uludağ University Journal of the Faculty of Engineering*, 24(2), 373-392. (in Turkish)

Tymrak BM, Kreiger M, Pearce JM (2014). Mechanical properties of components fabricated with open-source 3-D printers under realistic environmental conditions. *Materials & Design*, 58, 242-246.

Wang Y, Li X, Chen Y, Zhang C (2021). Strain rate dependent mechanical properties of 3D printed polymer materials using the DLP technique. *Additive Manufacturing*, 47, 102368.

Challenge Journal of Structural Mechanics

Research Article

Influence of the distance between vertical cylinders positioned in a row on the wind load on them

Lyubomir A. Zdravkov [a,*]

[a] *Department of Metal, Wood and Plastic Structures, University of Architecture, Civil Engineering and Geodesy (UACEG), Sofia 1046, Bulgaria*

ABSTRACT

The silos and vertical cylindrical tanks of small volumes are often built in batteries, at short distances between them. As a result of their close location, the wind load on them increases. In the European standard EN 1991-1-4:2005+A1:2010 exists a methodology for determining this increase, which is dependent on the ratio a/d, where a is the distance between the facilities and d is their diameters. Unfortunately, this methodology is applicable for ratios $a/d > 2.5$. In cases where the values are smaller, the standard transfers to the national annexes. In the available to the author annexes, including the Bulgarian one, there is nothing on the subject. Moreover, the necessary information could not be found in the public scientific literature. Only in the Australian/New Zealand standard AS/NZS 1170.2:2011 are written some simple rules for closely spaced vessels. To fill this gap, multiple models of closely spaced cylindrical bodies has been created by the author. A computer fluid simulation (CFD) program is used for this purpose. In the present study, the bodies are arranged in one row and the wind blows them perpendicularly. Through these computer models is determined how the wind load changes due to their proximity. In contrast to what is stated in EN 1991-1-4:2005+A1:2010, the dependence is not linear, and the influence of the close arrangement of the bodies decays much faster. On the other hand, this influence should be considered at much greater distances between bodies than stated in AS/NZS 1170.2:2011.

ARTICLE INFO

Article history:
Received 3 June 2024
Revised 19 August 2024
Accepted 26 August 2024

Keywords:
Vertical cylinder
Wind
Distance
Load
CFD analysis

1. Introduction

Silos and vertical cylindrical tanks of small volumes are often built in batteries, at short distances between them. As a result of their close location, the wind load on them increases. Some standards specify how this should be accounted for. For example, standard AS/NZS 1170.2:2011 states that grouped circular bins, silos and tanks with spacing between walls greater than two diameters shall be treated as isolated silos. Closely spaced groups with spacing less than 0.1 diameters shall be treated as a single structure for wind actions. For intermediate spacings, linear interpolation shall be used.

The European standard about wind load from 2005, EN 1991-1-4:2005, states that for vertical cylinders arranged in a row, the force factor k depends on the wind direction relative to the axis of the row and on the ratio of between distance a and diameter d, as shown in Table 1.

In the latter edition of the standard, EN 1991-1-4:2005+A1:2010, there is a change in how to determine the factor k, as is shown in Table 2.

In the available to the author National Annexes is written:

a) In the Bulgarian National Annex, BDS EN 1991-1-4:2005/NA:2011 – there are no defined values for the factor k when $a/d < 2.5$;

b) In the Danish National Annex, DS/EN 1991-1-4 DK NA:2015, is written only "Table 7.14 may underestimate the wind force for $a/b < 2.5$". I.e. the problem is here and it is clear, but there is no solution for it;

c) In the Singapore National Annex, NA to SS EN 1991-1-4:2009 – there are no additional information.

* *Corresponding author*. Tel.: +359-885-081-305 ; E-mail address: zdravkov_fce@uacg.bg (L. A. Zdravkov)
ISSN: 2149-8024 / DOI: https://doi.org/10.20528/cjsmec.2024.03.003

Table 1. Factor k for change of the wind load on vertical cylinders in a row arrangement according to EN 1991-1-4:2005, Table 7.14.

a/d	k	
$a/d < 3.5$	1.15	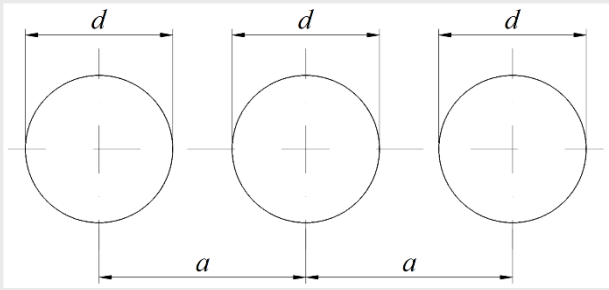
$3.5 < a/d < 30$	$\frac{210 - \frac{a}{d}}{180}$	
$a/d > 30$	1.00	

Table 2. Factor k for change of the wind load on vertical cylinders in a row arrangement according to EN 1991-1-4:2005+A1:2010, Table 7.14.

a/d	k	
$2.5 < a/d < 3.5$	1.15	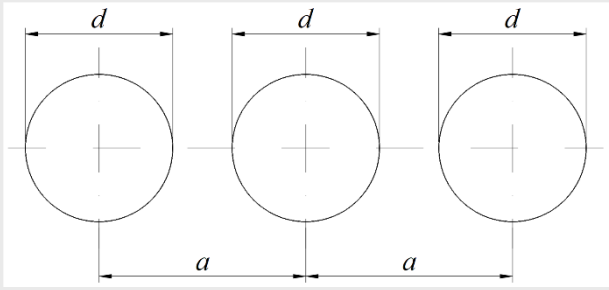
$3.5 < a/d < 30$	$\frac{210 - \frac{a}{d}}{180}$	
$a/d > 30$	1.00	

Note: for $a/d < 2.5$ the values of k may be given in the National Annex.

Macdonald et al. (1990) have studied in detail how the wind pressure changes over individual points in the central body of five closely spaced cylindrical bodies. Both the distance between the bodies and the angle of attack of the wind flow relative to the axis of the array of bodies were varied in their experimental models. Unfortunately, they did not look at how the summarized (total) wind load changes for the entire cylindrical body.

Except for the research above, no other useful information on the topic public scientific literature has been discovered by the author. To fill this gap, numerous models of closely spaced cylindrical bodies, where $a/d < 2.5$, see Tables 1 and 2, has been created. They are arranged in one row. A computer fluid simulation (CFD) program is used for this purpose. Through these numerical models is determined how the close position of the bodies changes the wind load on them.

2. Description of the Numerical Model

In the present study, the behaviour of the wind flow and the load generated by it was chosen to be analysed through computer simulation. Using the Workbench graphical interface of ANSYS (2024) and its Fluid Flow (CFX) module, multiple spatial models of site-built vertical cylinders were created. They are arranged in one row, perpendicularly to the wind flow. For bigger realism, their roofs are conical, with a height f = 50 mm, see Fig. 1.

The diameter of all cylindrical bodies is only one, d = 1,000 mm. In the models, the heights of the cylindrical bodies, their number, and the distance between them are changed. There are three heights of the cylindrical parts of the bodies – h = 2,500 mm, 5,000 mm and 7,500 mm. The other changes in the stacked cylindrical bodies are as follows:

a) Number of the cylinders – n = 1; 2; 3; 4 and 5, see Fig. 2;

b) The distance between their centres, see Tables 1 and 2, a = 1.1; 1.2; 1.5; 2; 3; 4; 5; 6; 7; 8, 9 and 10 m.

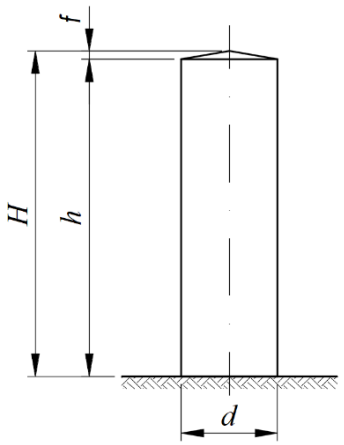

Fig. 1. Shape and dimensions of the examined bodies.

Spatial analysis was used in the present study. First, a cylindrical body is created, with the shape and dimensions shown in Fig. 1. Then it is multiplied. Parallelepiped-shaped wind tunnels have been created around the rows of cylinders, see Figs. 3 and 4. The boundaries of the wind tunnels are located at the following distances:

a) About the facilities with height h = 2,500 mm and 5,000 mm:
- Inlet of the fluid – at 30 m;
- Outlet of the fluid – at 60 m, i.e. the cylindrical bodies are located closer to the inlet of the wind tunnel than to the outlet, see Fig. 3;
- Vertical boundaries – at 30 m;
- "Roof" of the tunnel – at 30 m;
- "Bottom" of the tunnel – because the cylindrical bodies in the current simulations are placed on the ground, the distances between them and the "bottom" are equal to zero.

b) About the facilities with height h = 7,500 mm:
- Inlet of the fluid – at 45 m, see Fig. 4;
- Outlet of the fluid – at 90 m;
- Vertical boundaries – at 45 m;
- "Roof" of the tunnel – at 45 m;
- "Bottom" of the tunnel – the distances between the cylindrical bodies and the "bottom" are equal to zero.

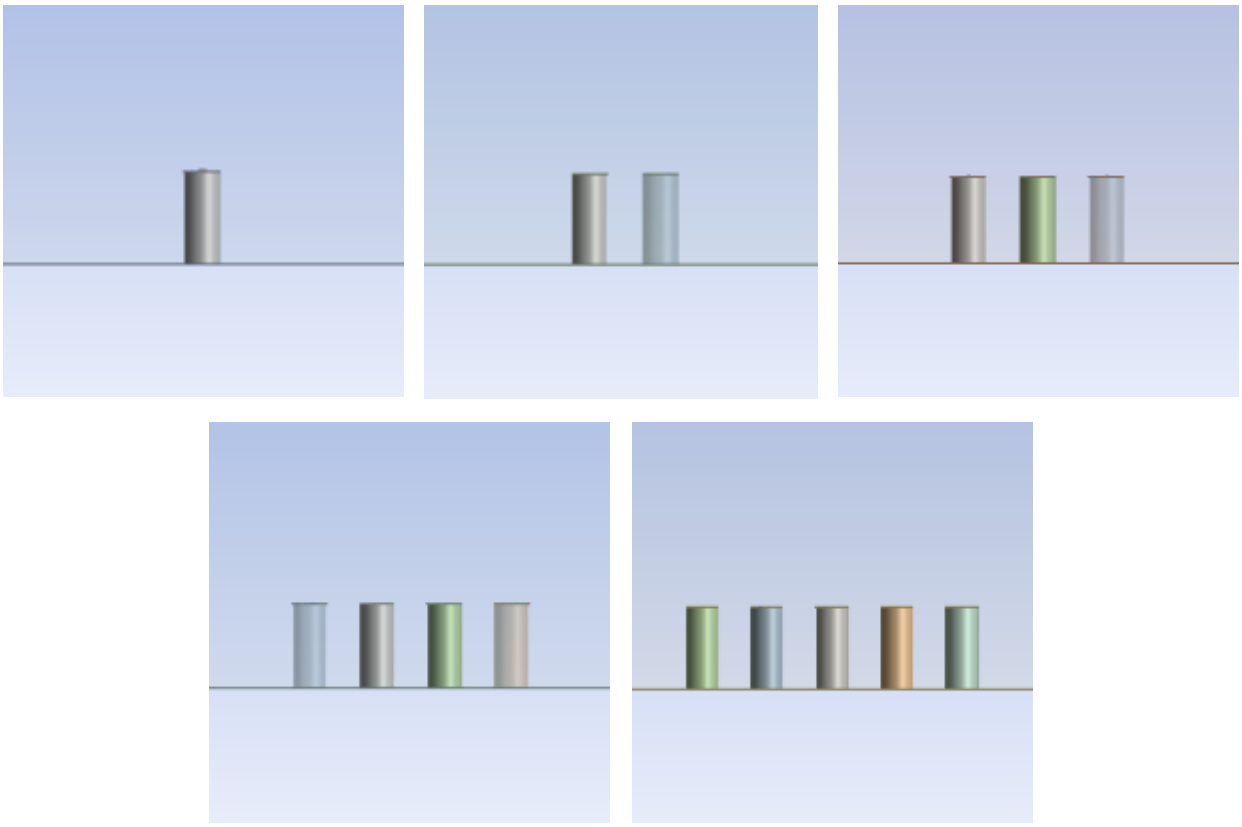

Fig. 2. Number and position of the examined bodies.

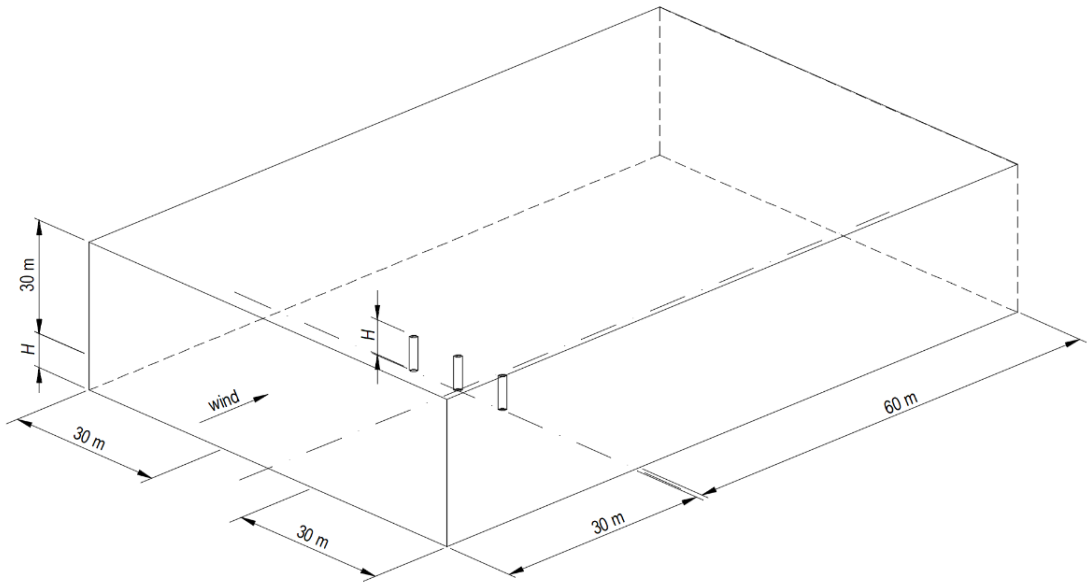

Fig. 3. Shape and dimensions of the wind tunnels
when heights of the cylindrical bodies are h = 2,500 mm and 5,000 mm.

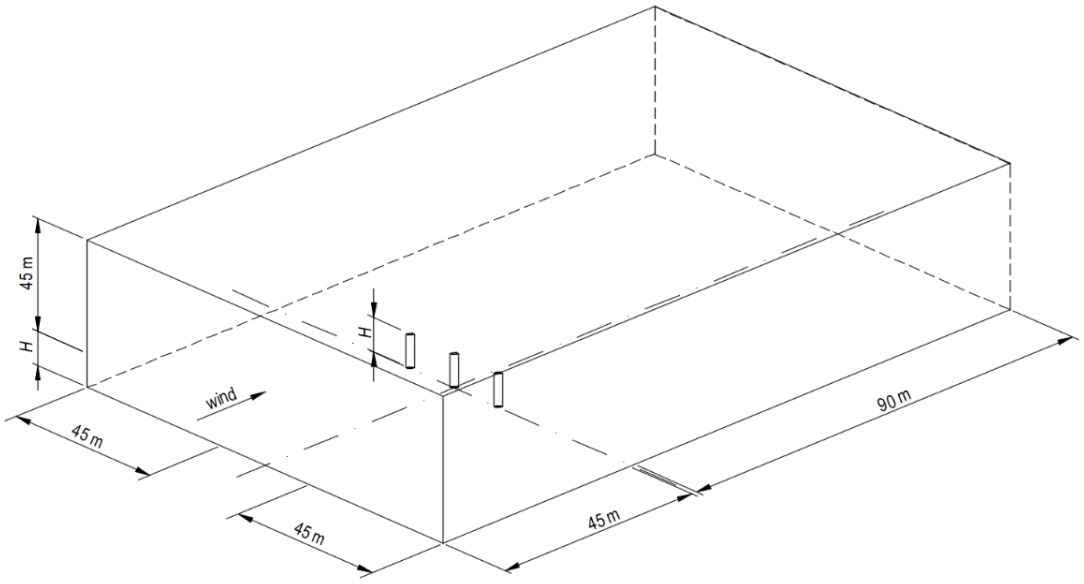

Fig. 4. Shape and dimensions of the wind tunnels when heights of the cylindrical bodies are h = 7,500 mm.

The determining of the above-written distances between the boundaries of the virtual wind tunnel and the facilities is based on the principle that airflow adjacent to the bodies should not be affected, see Rusev et al. (2012a) and Pantusheva et al. (2022). Accepted distances are bigger than the requirements of Tominaga et al. (2008), as follows:

- The top/side boundary should be set 5H or more away from the obstacle, where H is the whole height of the bodies in the current research ($H = h+f$, see Fig. 1);
- The outlet boundary should be set at least 10H behind the obstacle.

For facilities where h = 5,000 mm and 7,500 mm their total height is H = 5,050 mm and 7,550 mm respectively. In other words, the accepted distances are almost 6H and 12H, like the simulations of Hillawaere et al. (2013, 2015).

At the same time, to avoid heavy computer solutions and save computational time, the maximum number of finite elements is maintained within reasonable limits. To optimize their mesh, it is significantly refined in the area around the facilities, see Fig. 5, and is coarse to the periphery, as is done in Rusev et al. (2012b). The maximum size of the finite elements of the air is limited to:

a) Elements in direct contact with the cylindrical bodies – 100 mm;
b) Elements in direct contact with the “bottom” of the wind tunnel – 500 mm;
c) All other elements – 1,000 mm.

The "Linear" option was used when creating the mesh finite elements, as a result of which nodes in the middle of their edges are not preserved. This approach reduces the required computational time. The finite elements are "Tetrahedrons", with four nodes each. The algorithm for creating the mesh is "patch conforming", i.e. it starts from the edges and surfaces of bodies. This approach guarantees a "clean" mesh and high accuracy of the solution.

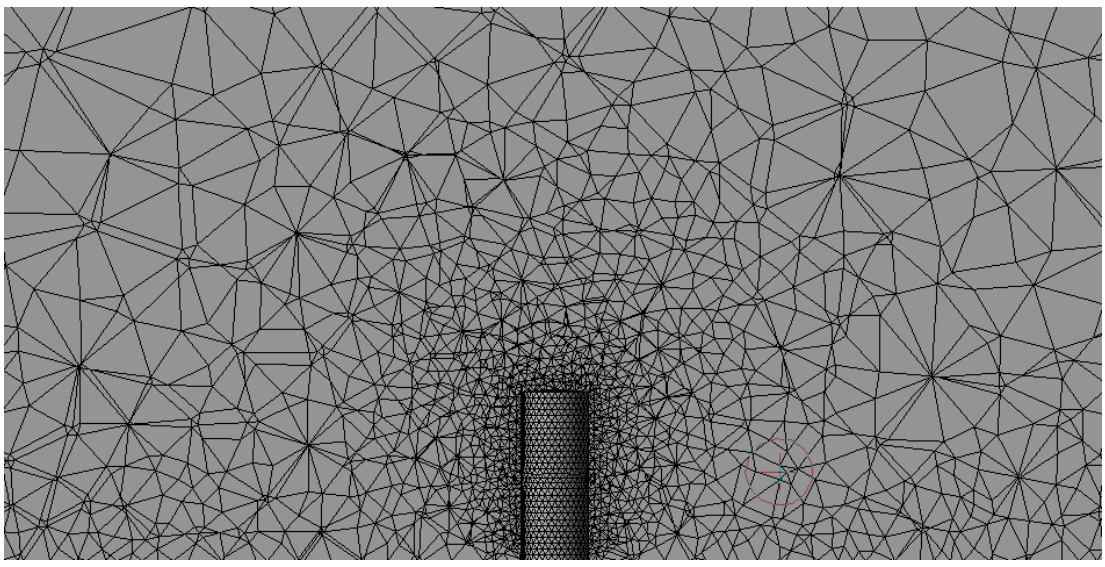

Fig. 5. Refinement of the mesh around the circular bodies.

Steady-state analysis type is used in a Fluid Flow (CFX) module. k-ε model, part of the Reynolds-averaged Navier Stokes (RANS) family, is used to simulate the turbulent flow of the fluid around the bridges. According to Agyropulos and Markatos (2015), they look like as:

$$\frac{\partial \overline{u_i}}{\partial t} + \frac{\partial (\overline{u_i}\,\overline{u_j})}{\partial x_j} = -\frac{1}{\rho}\frac{\partial \bar{p}}{\partial x_i} + \nu \frac{\partial^2 \overline{u_i}}{\partial^2 x_j} - \frac{\partial \left(\overline{u_i'}\,\overline{u_j'}\right)}{\partial x_j} \quad (1)$$

where u_i is the mean speed of the fluid; $\overline{u_i'}$ is the change of the speed; ρ is the density of the fluid; ν is the kinematic viscosity; t is the time; $\bar{p}$ is the pressure of the fluid; and $u_i' u_j' = \tau_{ij}$ is the tensor of the stresses of Reynolds.

In analogy to molecular viscous stresses, Reynolds stresses can be represented by Markatos (1986) as:

$$\tau_{ij} = \overline{u_i'}\,\overline{u_j'} = \frac{2}{3}k\delta_{ij} - \nu_t\left(\frac{\partial \overline{u_i}}{\partial x_j} + \frac{\partial \overline{u_j}}{\partial x_i}\right) \quad (2)$$

where k is the kinetic turbulence energy; and $\nu_t = \mu_t/\rho$ is the turbulence or eddy (kinematic) viscosity.

In the models with one equation, according to Launder and Sharma (1974), ν_t is accounted by the expression:

$$\nu_t = C_{\nu 1}\sqrt{kL} \quad (3)$$

in which $C_{\nu 1}$ is a dimensionless parameter.

A two-equation model, such as the used here standard k–ε model, uses differential equations to calculate the characteristic velocity, on the length scale L, and then evaluates the value of ν_t by the following equation, see Markatos (1986):

$$\nu_t = C_\mu \frac{k^2}{\varepsilon} \quad (4)$$

where $C_\mu = 0.09$; and ε is the turbulence dissipation rate.

These RANS equations are an adequate representation of the wind tunnel's reality, Baklanov et al. (2007). Accepted turbulence has a medium (5%) intensity. No combustion and thermal radiation. The used fluid is an air-ideal gas with a temperature of 25 °C. Its speed at the inlet domain of the tunnel is constant in height and has a value of v = 25 m/s. Flow regimes in the outlet and opening domains are subsonic, with a relative pressure of 0 Pa. Flow direction is normal to boundary conditions for the domain opening. The domain of cylindrical bodies is a no-slip smooth wall. The surface of the terrain under the bridge is perfectly smooth, too (Zdravkov 2022).

Unlike the research of Yu et al. (2011), main wind flow is horizontal there, i.e. the angle of attack is 0°. The direction of the approaching wind is perpendicular to the axes of the row of cylinders.

During its movement, the wind flows around the facilities, see Fig. 6a, which leads to the occurrence of pressure on their surfaces, see Fig. 6b. As a result, horizontal forces are generated at the base of the cylindrical bodies and they can be accounted. Considering the force at the base of an isolated (independent) cylinder and comparing it with the forces at the bases of multiple bodies united in a group, can determine the influence of the distance between the bodies, using Eq. (5):

$$k = \frac{F_{h,i}}{F_{h,1}} \quad (5)$$

where $F_{h,i}$ is the horizontal force at the base of the i-th cylindrical body of the group, accounted in the direction of the wind flow; and $F_{h,1}$ is the accounted in the direction of the wind flow horizontal force at the base of the isolated (independent) cylinder.

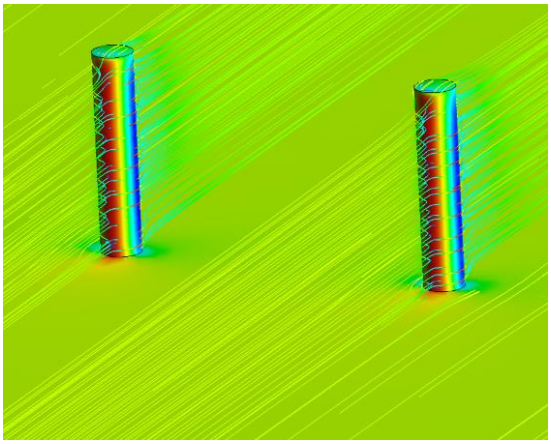

(a) wind flow around the facilities

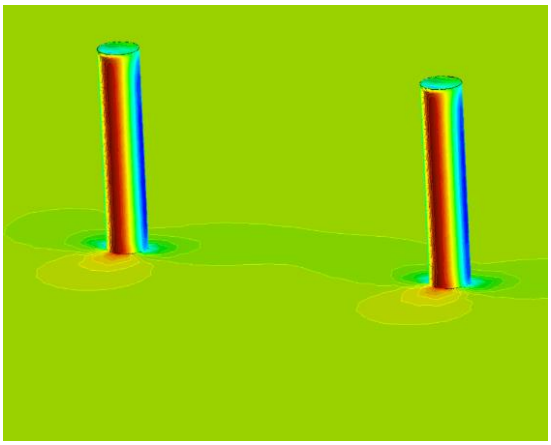

(b) pressure on surfaces of the bodies

Fig. 6. Wind flow around the cylindrical bodies and the resulting pressure on their surfaces.

3. Results and Discussion

The shearing force $F_{h,i}$ in the base of every one cylindrical body in the group is obtained during the research. Analogical data $F_{h,1}$ is accounted for the isolated (independent) cylinders. The values of factor k are calculated, using Eq. (5). They are shown graphically in Figs. 7–9, where: a is the axial distance between the cylindrical bodies, see Table 1 and 2; and d = 1,000 mm is the diameter of the bodies in the research.

The numerically obtained values for the factor k are compared with those, determined analytically, according to the methodology of EN 1991-1-4:2005+A1:2010, see yellow line in Figs. 7–9.

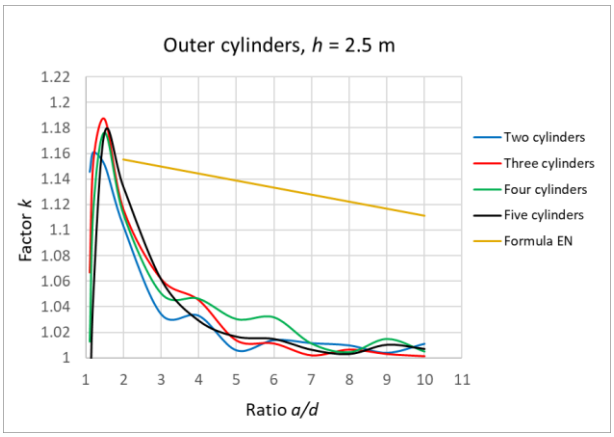

(a) at outer cylinders

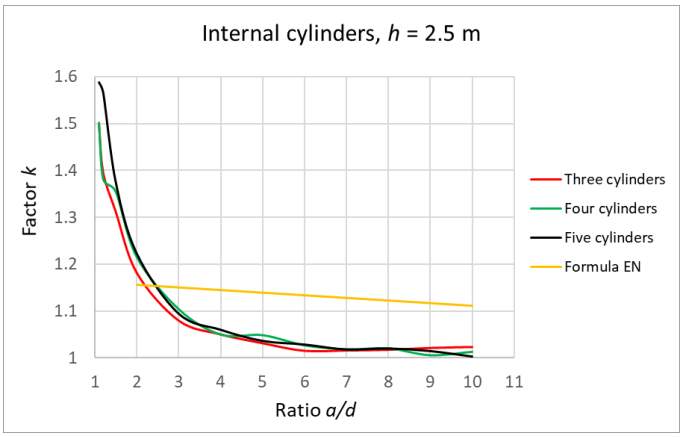

(b) at internal cylinders

Fig. 7. Influence of the distance between cylindrical bodies with a high h = 2.5 m on the total wind load on them.

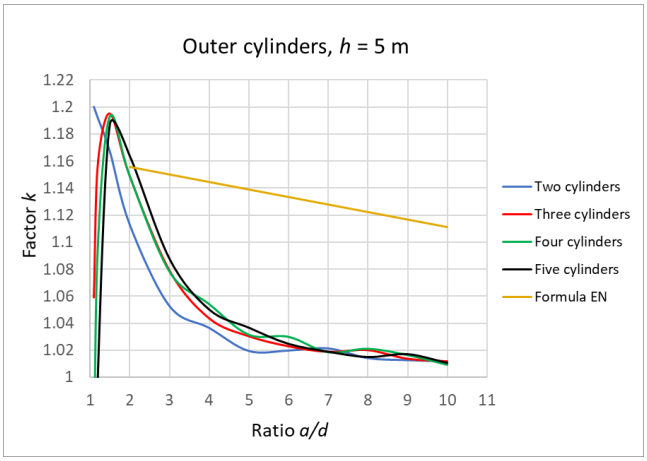

(a) at outer cylinders

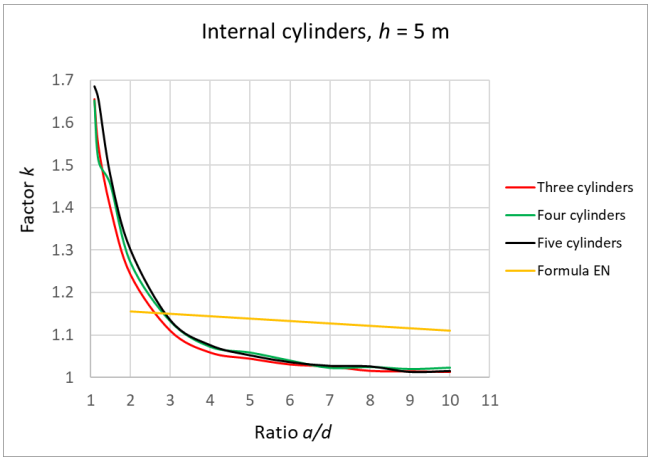

(b) at internal cylinders

Fig. 8. Influence of the distance between cylindrical bodies with a high h = 5 m on the total wind load on them.

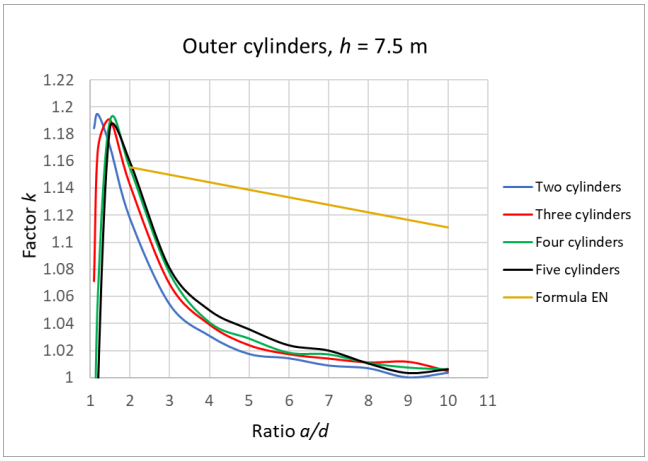

(a) at outer cylinders

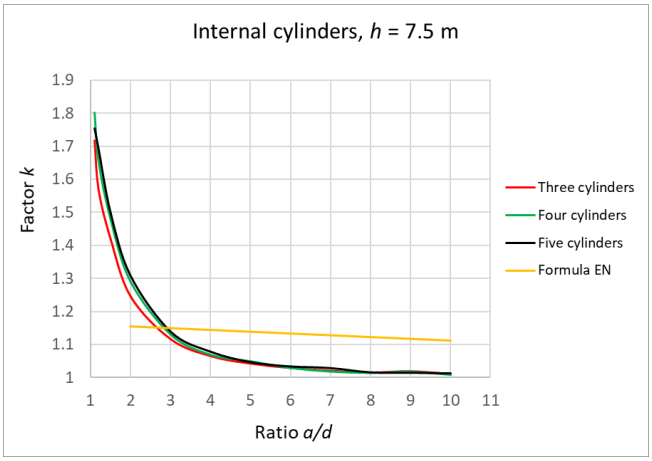

(b) at internal cylinders

Fig. 9. Influence of the distance between cylindrical bodies with a high h = 7.5 m on the total wind load on them.

Analyzing the graphs above within the framework of the present study, where the maximum number of cylindrical bodies in a row is five and the axial distance between them is in the interval $a = (1.1 \div 10) \cdot d$, the following impression is made:

a) When wind blows perpendicularly to the axis of the row, there is a difference in the wind load on the outer and internal bodies. The shearing forces in the bases are smaller at the outer bodies and bigger at the internal ones;

b) The amplification of the wind load is more significant for bodies with larger values of the height-to-diameter ratio (h/d);
c) The wind load on the cylindrical bodies decreases as the distance between them increases. The dependence here is non-linear, in contrast to the linear expression, specified in standard EN 1991-1-4:2005+A1:2010;
d) For outer cylindrical bodies, the coefficient $k < 1.2$, regardless of how close they are to each other. I.e., for them can be assumed factor $k = 1.2$ within the limits $1.1 \leq a/d < 2.5$;
e) For internal bodies, the factor k can be taken as follows:
- $k = 1.8$ within the limits $1.1 \leq a/d < 1.5$;
- $k = 1.55$ within the limits $1.5 \leq a/d < 2.0$;
- $k = 1.35$ in the limits $2.0 \leq a/d < 2.5$;

f) The maximum value of the factor $k \approx 1.027$ at a ratio $a/d = 8$, i.e. the overload is only 2.7% compared to an isolated cylinder. The coefficient k is even smaller for values of $a/d > 8$. It is therefore very likely the specified in the standard EN 1991-1-4:2005+A1:2010 requirement to consider the influence of closely spaced cylindrical bodies at $a/d < 30$, is too strict. On the other hand, it is quite possible that the statement in the Australian and New Zealand standard AS/NZS 1170.2:2011, that at distances greater than twice their diameter they should be considered as isolated (separate) facilities, is overly optimistic.
g) At the current stage of the research it appears that when the ratio $a/d > 8$, the increase in the wind load is negligibly small and does not necessary to be considered.

4. Conclusions

The European standard EN 1991-1-4:2005+A1:2010 does not specify a methodology for determining the increase in wind load at ratio $a/d < 2.5$, see Tables 1 and 2. In the available to the author national annexes, including the Bulgarian one, BDS EN 1991-1-4:2005/NA:2011, recommendations on the subject do not exist, too. In an attempt to find the information he needed, the author first surveyed the available scientific literature on the topic. After failing to find the necessary data, a parametric computer study was conducted. Many numerical models of closely spaced cylindrical bodies, has been created, using the ANSYS Workbench graphical interface and its Fluid Flow (CFX) computer simulation module. The following conclusions can be drawn from the research:

- The reduction of the effect of the mutual influence of closely located bodies is non-linear, in contrast to the linear dependence specified in the standard EN 1991-1-4:2005+A1:2010. This requires the written in the standard methodology to be refined;
- The mutual influence of the bodies due to wind load on them decreases much faster, compared to what is indicated in EN 1991-1-4:2005+A1:2010. On the other hand, this influence should be considered at much greater distances between bodies than stated in AS/NZS 1170.2:2011. I.e. here both standards should be refined;
- The following values could be assumed for the factor k, until more research is done on the subject:
  - For outer bodies – $k = 1.2$ within the limits $1.1 \leq a/d < 2.5$;
  - For internal bodies:
    $k = 1.8$ within the limits $1.1 \leq a/d < 1.5$;
    $k = 1.55$ within the limits $1.5 \leq a/d < 2.0$;
    $k = 1.35$ in the limits $2.0 \leq a/d < 2.5$;

Acknowledgements
None declared.

Funding
The author received no financial support for the research, authorship, and/or publication of this manuscript.

Conflict of Interest
The author declared no potential conflicts of interest with respect to the research, authorship, and/or publication of this manuscript.

Data Availability
The datasets created and/or analyzed during the current study are not publicly available, but are available from the corresponding author upon reasonable request.

REFERENCES

Agyropulos C, Markatos N (2015). Recent advances on the numerical modelling of turbulent flows. *Applied Mathematical Modelling*, 39, 693–732.

ANSYS® v.2024 R1 (2024). Documentation. Ansys Inc., Canonsburg, PA, the USA.

AS/NZS 1170.2 (2011). Structural Design Actions. Part 2: Wind actions. Standards Australia Limited / Standards New Zealand. ISBN 978-0-7337-9805-4.

Baklanov A, Barmpas P, Bartzis J, Batchvarova E, et al. (2007). Best Practice Guideline for the CFD Simulation of Flows in the Urban Environment. *edited by Franke J, Hellsten A, Schlunzen H and Carissmo B*. COST Action 732, Brussels, Belgium. ISBN: 3-00-018312-4.

BDS EN 1991-1-4:2005/NA (2011). Eurocode 1: Actions on structures – Part 1-4: General actions – Wind actions. National annex to BDS EN 1991-1-4:2005. Bulgarian Institute for Standardization, Sofia.

DS/EN 1991-1-4 DK NA (2015). Eurocode 1: Actions on structures – Part 1-4: General actions – Wind actions. National annex to DS/EN 1991-1-4. Danish Standards Foundation, København.

EN 1991-1-4 (2005). Eurocode 1: Actions on structures – Part 1-4: General actions – Wind actions. European Committee for Standardization, Brussels.

EN 1991-1-4:2005+A1 (2010). Eurocode 1: Actions on structures – Part 1-4: General actions – Wind actions. European Committee for Standardization, Brussels.

Hillewaere J, Degroote J, Rezayat A, Vanlanduit S, Lombaert G, Vierendeels J, Degrande G (2013). Numerical investigation of wind induced ovalling vibrations in silo groups. *4th ECCOMAS Thematic Conference on Computational Methods in Structural Dynamics and Earthquake Engineering*, Greece.

Hillewaere J, Degroote J, Lombaert G, Vierendeels J, Degrande G (2015). Wind-structure interaction simulations of ovalling vibrations in silo groups. *Journal of Fluids and Structures*, 59, 328-350.

Launder B, Sharma B (1974). Application of the energy dissipation model of turbulence to the calculation of flow near a spinning disk. *Letters in Heat and Mass Transfer*, 1, 131-138.

Macdonald P, Holmes J, Kwok K (1990). Wind loads on circular storage bins, silos and tanks. II. Effect of grouping. *Journal of Wind Engineering and Industrial Aerodynamics*, 34, 77-95.

Markatos N (1986). The mathematical modelling of turbulent flows. *Applied Mathematical Modelling*, 10(3), 190-220.

NA to SS EN 1991-1-4 (2009). Eurocode 1: Actions on structures – Part 1-4: General actions – Wind actions. National annex to SS EN 1991-1-4:2009. Standards Council of Singapore, Singapore.

Pantusheva M, Mitkov R, Hristov PO, Petrova-Antonova D (2022). Air pollution dispersion modelling in urban environment using CFD: A systematic review. *Atmosphere*, 13, 1640.

Rusev I, Tanev T, Dinev D (2012a). Numerical study of wind actions on tall buildings with ANSYS CFX and comparison with EN1991-1-4. Proceedings of XII International *Scientific Conference* VSU'2012, Sofia, vol. 1, pp. 83-88. (in Bulgarian)

Rusev I, Dinev D, Tanev T (2012b). Numerical study of wind actions on nearby tall buildings. Proceedings of *International Jubilee Scientific Conference UACEG'2012*, Sofia, pp. 15-17. (in Bulgarian)

Tominaga Y, Mochida A, Yoshie R, Kataoka H, Nozu T, Yoshikawa M, Shirasawa T (2008). AIJ guidelines for practical applications of CFD to pedestrian wind environment around buildings. *Journal of Wind Engineering and Industrial Aerodynamics*, 96(10-11), 1749-1761.

Yu M, Liao H, Li M, Ma C, Luo N, Liu M (2011). Study on static wind loading coefficients of suspension bridge, based on CFD simulation and wind tunnel test. *Applied Mechanics and Materials*, 66-68, 334-339.

Zdravkov L (2022). Wind loads on girder bridges. *Challenge Journal of Structural Mechanics*, 8(1), 9-16.

Challenge Journal of Structural Mechanics

Research Article

Optimization of mechanical properties in lime-based composites using the Taguchi method

Bekir Güney [a,*], Sadık Alper Yıldızel [b]

[a] *Department of Motor Vehicles and Transportation Technologies, Karamanoğlu Mehmetbey University, 70100, Karaman, Türkiye*
[b] *Department of Civil Engineering, Karamanoğlu Mehmetbey University, 70100 Karaman, Türkiye*

ABSTRACT

Global warming is widely recognized as one of the most pressing issues of our time. One of the primary contributors to this phenomenon is the emission of CO_2, which significantly exacerbates global warming. Today, the production and industry of cement stand out as leading sources of carbon emissions. Consequently, the scientific community is actively researching solutions to reduce cement usage. Some of these efforts focus on alternative binders such as silica fumes and lime. In this study, the goal is to enhance silica fume and lime binder composites, optimizing them for both refractory and insulating properties using the Taguchi optimization method. The results indicate significant improvements in compressive and flexural strengths, which were further validated through testing. The highest compressive strength achieved was 11.97 MPa, while the maximum flexural strength reached 0.34 MPa. This research underscores the potential of alternative binders in mitigating the environmental impact of cement production while enhancing material performance in various applications.

ARTICLE INFO

Article history:
Received 10 July 2024
Revised 26 August 2024
Accepted 5 September 2024

Keywords:
Silica fume
Lime
Insulation
Taguchi
Optimization

1. Introduction

Today, climate change occurring as a result of both anthropogenic and natural effects significantly worsens human and environmental security (Karanafti et al. 2022). People spend most of their time in buildings, both in their daily and working lives. These buildings are expected to have comfort features that will not threaten human health and safety. Especially as a result of anthropogenic effects, a large amount of various waste products is released into the environment in industrial sectors. These products cause global warming, which is a major environmental problem, by releasing greenhouse gases such as carbon dioxide, especially disposal problems. The construction industry is one of them (Kosse et al. 2016).

It is estimated that buildings consume more than 45% of global energy consumption (Rashad et al. 2022a) and this figure is expected to rise in the coming years (Rashad et al. 2022b). Effectively managing scarce energy resources has become a top priority worldwide, particularly as energy demand continues to grow rapidly. Currently, achieving comfort in energy-efficient buildings involves using insulation materials that are not only environmentally friendly but also energy-saving, thanks to their thermal and mechanical properties. These modern materials are replacing traditional options, enabling buildings to maintain comfort while reducing energy consumption and environmental impact (Van Nguyen 2023).

Thermal insulation materials are crucial for maintaining comfortable indoor temperatures for both heating and cooling while preserving the natural state of living organisms and objects. These materials are broadly categorized into two main types: inorganic and organic. Inorganic insulation materials, such as silica fume (SF) based geopolymers, are extensively used in the construction industry. The use of mineral additives such as mi-

* *Corresponding author*. Tel.: +90-338-226-2000 ; E-mail address: guneyb@kmu.edu.tr (B. Güney)
ISSN: 2149-8024 / DOI: https://doi.org/10.20528/cjsmec.2024.03.004

crosilica, also known as silica fume, in cementitious systems has positive effects both environmentally and economically. It helps fill voids and exhibits a partial binding effect, enhancing the overall performance of the material (Yorulmaz et al. 2021; Oltulu and Şahin 2013). They are preferred due to their low flammability and non-toxic properties. Despite having higher thermal conductivity compared to organic insulation materials, inorganic options like geopolymers offer superior mechanical strength and environmental durability (Rashad et al. 2024). It has been stated that geopolymers offer numerous advantages, including superior mechanical properties (Mahmoodi et al. 2022), high resistance to elevated temperatures (Çelikten et al. 2020), and resistance to acid (Thokchom et al. 2009) and sulfate effects (Bhutta et al. 2013), along with environmentally friendly characteristics (Alakara et al. 2022). These characteristics make them highly suitable for applications where fire safety and longevity are critical considerations.

Alkaline liquid and pozzolanic materials are used to bond geopolymer material components. Inorganic mineral additive materials such as SF, metakaolin, slag and fly ash, rich in silica (Si) and aluminum (Al), are preferred as pozzolanic materials (Duxson et al. 2007; Tho-In et al. 2012). Aluminum silicates in pozzolanic materials enable the production of high-performance geopolymer materials in terms of their physical and mechanical properties through polymerization reaction (Zakka et al. 2021). Additionally, calcium hydroxide (lime), a weak alkali with a high calcium content, can be incorporated into components to improve the setting time and early strength of such geopolymers (Das et al. 2020). Additionally, by adding waste materials such as SF, additional silicate is included in the geopolymer system (Bajpai et al. 2020). The increase in the silicate/aluminate ratio in geopolymers increases the strength of the produced composite materials (Jena et al. 2019; Okoye et al. 2016).

SF is a refractory material that is a by-product with a high level of pozzolanic properties, consisting of glassy silica (SiO_2) particles with an amorphous crystalline structure, micrometric dimensions, during the manufacturing of silicon or iron ferrosilicon alloys (Al-Amoudi et al. 2007; Koca 1996; Liu et al. 2009). In the production process, it is obtained by reducing high purity quartzite with coal in electric arc furnaces at a temperature of approximately 2000 °C (Golafshani and Behnood 2019).

When SF, lime and water are mixed in certain proportions, a hydration reaction occurs. The reason why SF shows high pozzolanic activity is attributed to its very large surface area and amorphous character (Abo-El-Enein et al. 1996). The molecular calcium silicate hydration (C-S-H) reaction caused by SF and water depending on the CaO/SiO_2 ratio may differ (Cohen and Bentur 1988).

Basic hydration occurs in the process of dissolution of alite (C_3S) and belite (C_2S) in the formation of C-S-H and calcium hydroxide (CH) precipitation. While CH is a known crystalline phase (Petch 1961), C-S-H gel is a natural nanostructured material (Wang et al. 2024). C-S-H precipitates as a filling material and shows a pozzolanic effect. Thanks to this feature, the voids of the geopolymer material decrease and its stability improves (Muller et al. 2015). The highly pozzolanic nature of SF increases its capacity to react with free lime during hydration. SF forms C-S-H gels that provide density, strength, impermeability and durability in the geopolymer produced as a result of the CH reaction (Guleria and Salhotra 2016; Rodrigues et al. 2013). It also provides early strength and durability by being activated through a highly alkaline solution and thermal curing (Koca 1996). Thermal and mechanical properties can be further improved by selecting the most optimum ratios of SF, free lime and water (Al Zaidi et al. 2019).

Thermal insulation materials have different advantages. These include thermal conductivity, perforation gap, site adaptability, workability, mechanical strength, fire protection, smoke emission during fire, durability, resistance to climate variations, resistance to freeze/thaw cycles, water resistance, costs, biocompatibility, toxicity and environmental impacts (Güney 2019). In addition, high thermal protection, comfortable insulation and low operating costs are expected from these materials. Although there are many studies in the literature on improving concrete and its properties, there is limited information on the combined use of silica fume, free lime and water and its optimization with the Taguchi method.

Considering the diminishing material resources and the environmental damage caused by waste, the conversion of valuable materials such as silica fume into economic value is of great importance on a global scale. In this study, it was aimed to recycle silica fume, which is abundant in Türkiye as ferrosilicon and silicon ferrochrome production flue dust waste, into the economy in an environmentally friendly way. In the present study, the mechanical, physical and microstructural properties of the samples produced from different amounts of high temperature resistant silica fume, water and free lime mixture were investigated. The effects on sound permeability, thermal conductivity and water absorption of all samples produced were investigated. These materials were experimentally characterized using standard methods according to the relevant standards. It is clear that the insulation material produced using waste silica fume and lime shows promising results in terms of microstructure, physical and chemical properties. However, considering the constraints of limited resources and the imperative of sustainability, the importance of studying inorganic waste materials such as SF and lime greatly increases. In the present study, the effect of design variables on the physical and mechanical properties of SF with lime was optimized by Taguchi method and the relationships between the design variables were determined. Since this study is a first in this respect, it is believed that it will shed light on future optimization studies.

2. Materials and Method

2.1. Experimental studies

Within the scope of this study, detailed results of the experimental studies to be designed and optimized with Taguchi can be obtained from the previous study (Güney

2019). Compressive tests were performed on 28-day specimens according to TS EN 12390-3 (2019) and flexural tests were performed according to TS EN 12390-5 (2009). Three specimens were produced for each test and the arithmetic averages of the test results were considered.

2.2. Experimental design and optimization studies

Experimental design and optimization studies were carried out with the Taguchi method. Comprehensive results can be obtained with a small number of experiments using this technique (Calis et al. 2021; Gao et al. 2021). Silica fume content (SD), lime content (LM), and water binder ratio (WB) were taken as input parameters and compressive and flexural strengths were designed and optimized. Signal-to-noise (S/N) ratios were applied as 'bigger is better' for flexural and compressive strength evaluations. In addition, the contribution of each factor to the strengths was determined by ANOVA. During the experimental design, the number of experiments was reduced to 27 by Taguchi optimization. The flow diagram of the applied method is presented in Fig. 1. The experimental design proposed by Taguchi method is as shown in Table 1.

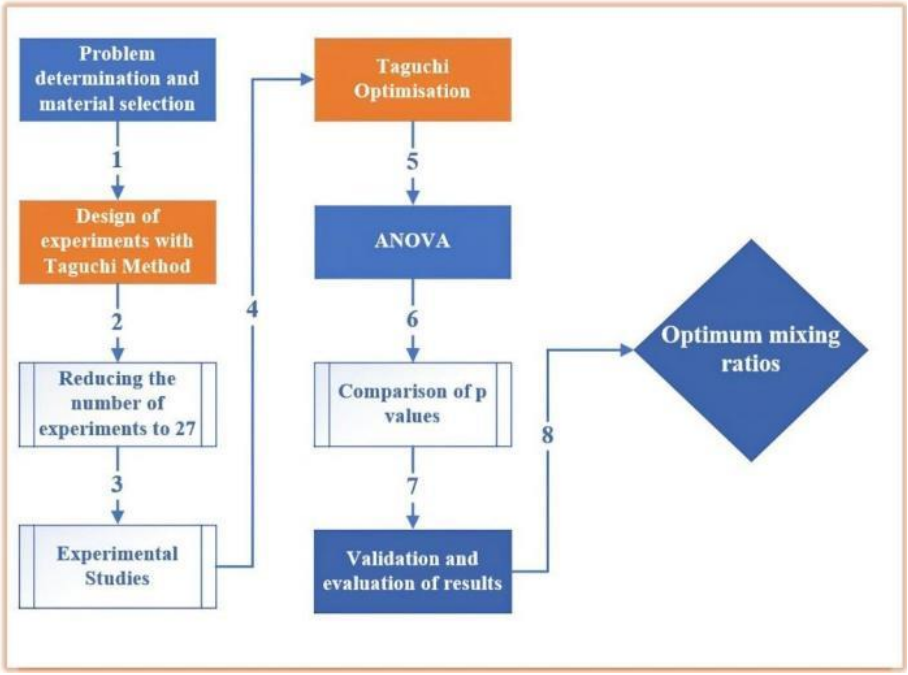

Fig. 1. Flow diagram of design and optimization studies.

Table 1. Mixing proportions of composites.

Mixture code	SD (%)	KM (%)	WB	BD (MPa)	ED (MPa)
K_1	59.14	40.86	0.80	9.21	0.25
K_2	59.14	40.86	0.80	9.18	0.25
K_3	59.14	40.86	0.80	9.23	0.25
K_4	59.14	48.22	0.82	9.32	0.25
K_5	59.14	48.22	0.82	9.28	0.25
K_6	59.14	48.22	0.82	9.34	0.25
K_7	59.14	55.76	0.90	8.47	0.23
K_8	59.14	55.76	0.90	8.42	0.23
K_9	59.14	55.76	0.90	8.45	0.23
K_{10}	51.68	40.86	0.82	11.54	0.31
K_{11}	51.68	40.86	0.82	11.47	0.31
K_{12}	51.68	40.86	0.82	11.51	0.31
K_{13}	51.68	48.22	0.90	11.79	0.32
K_{14}	51.68	48.22	0.90	11.81	0.32
K_{15}	51.68	48.22	0.90	11.74	0.31
K_{16}	51.68	55.76	0.80	8.81	0.24
K_{17}	51.68	55.76	0.80	8.79	0.24
K_{18}	51.68	55.76	0.80	8.85	0.24
K_{19}	44.24	40.86	0.90	8.54	0.23

Table 1. (continued)

Mixture code	SD (%)	KM (%)	WB	BD (MPa)	ED (MPa)
K_{20}	44.24	40.86	0.90	8.47	0.23
K_{21}	44.24	40.86	0.90	8.43	0.23
K_{22}	44.24	48.22	0.80	8.91	0.24
K_{23}	44.24	48.22	0.80	8.83	0.24
K_{24}	44.24	48.22	0.80	8.87	0.24
K_{25}	44.24	55.76	0.82	9.21	0.25
K_{26}	44.24	55.76	0.82	9.11	0.24
K_{27}	44.24	55.76	0.82	9.17	0.25

3. Results and Discussion

The Taguchi design and optimization results that will maximize the compressive strength are as given in Fig. 2. According to the optimization results, the recommended values for SD, KM and S/B are 51.68, 48.22 and 0.82, respectively. These results are in line with similar studies (Al-Waked et al. 2023; Ayasgil et al. 2022; Kang et al. 2019).

The optimum flexural strength achieved by the Taguchi design is shown in Fig. 3. Hence, the suggested values for SD, KM, and S/B are 51, 68, 48, 22, and 0.82, respectively. The achieved limitations fall within the range of values consistently reported in previous similar research. (Kaya et al. 2023; Malathy et al. 2022).

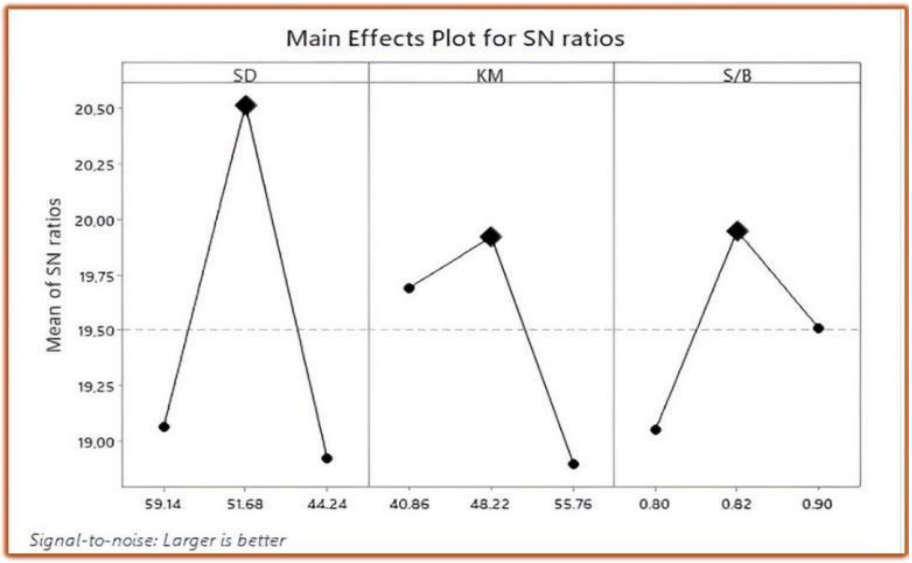

Fig. 2. Taguchi design results for compressive strength.

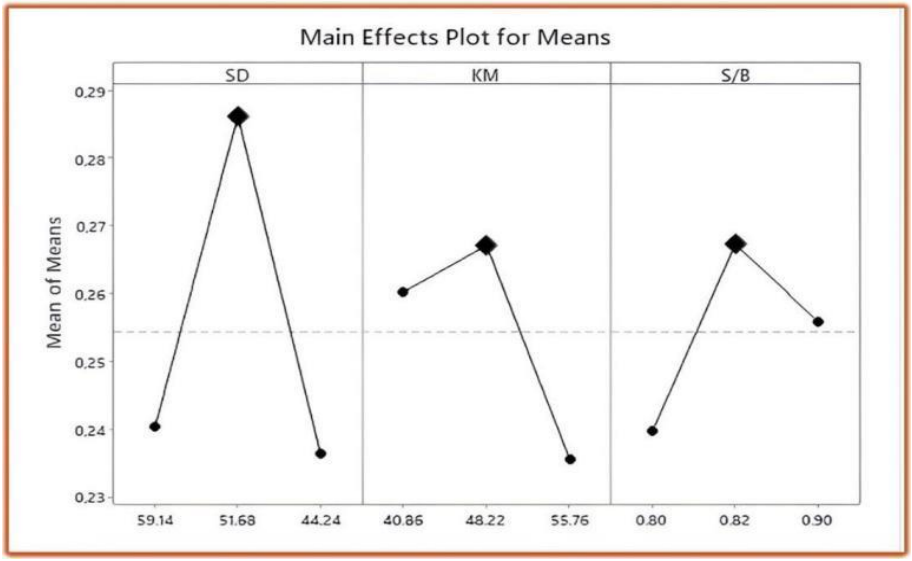

Fig. 3. Taguchi design results for flexural strength.

The ANOVA results within the compressive strength optimization studies are as shown in Table 2. According to the relevant table, since the "p" values of all components are less than 0.005, it is concluded that they have an effect on compressive strength (Yıldızel and Çalış 2019; Yildizel et al. 2022).

The ANOVA results of flexural strength are presented in Table 3. Accordingly, the p values for SD, KM and WB are 0.000, 0.001 and 0.004, respectively, and since all of them are less than 0.005, it is concluded that there is an effect on flexural strength.

The material quantities recommended by Taguchi design for SD, KM and S/B (51.68, 48.22 and 0.82) were used in the verification casting and the results obtained are as presented in Table 4. According to these results, higher compressive and flexural strengths were obtained as expected.

Table 2. ANOVA results for compressive strength design.

Source	DF	Adj SS	Adj MS	F	p
SD	2	19.2797	9.63983	30.02	0.000
KM	2	6.9185	3.45923	10.77	0.001
S/B	2	4.8221	2.41103	7.51	0.004
Error	20	6.4226	0.32113		
Lack of fit	2	6.3968	3.19841	2231.45	0.000
Pure error	18	0.0258	0.00143		
Total	26	37.4428			

Table 3. Flexural strength design ANOVA results.

Source	DF	Adj SS	Adj MS	F	p
SD	2	0.01379	0.006895	30.02	0.000
KM	2	0.0049	0.002474	10.77	0.001
S/B	2	0.0035	0.001724	7.51	0.004
Error	20	0.0046	0.000230		
Lack of fit	2	0.0046	0.002288	2231.45	0.000
Pure error	18	0.000018	0.000001		
Total	26	0.026781			

Table 4. Validation test results.

Type of experiment	Average test result (MPa)
Compressive strength (28 days)	11.97
Flexural strength (28 days)	0.34

4. Conclusions

In this study, optimization of construction materials produced using silica fume and lime using Taguchi method and validation of the obtained results were carried out. SD, KM and S/B quantities were considered as input values, while compressive and flexural strengths were taken as output values. The evaluations made in the light of the results obtained can be summarized as follows:

- According to the ANOVA results, each of the parameter's SD, KM and S/B are of great importance in compressive and flexural strength optimization studies.
- The values that maximize the compressive and flexural strengths were suggested by Taguchi optimization as 51.68%, 48.22% and 0.82% for SD, KM and S/B, respectively.
- According to the validation test results, the maximum BD was increased to 11.97 MPa and the maximum ED was increased to 0.34.

In future studies, further enhancement of Bulk Density (BD) and Elasticity (ED) values could be pursued using alternative optimization techniques. Exploring these different approaches may yield more refined control over these properties, leading to improved material performance and broader applications. By employing advanced optimization methods, it is possible to achieve even greater precision in tuning the physical and mechanical characteristics of the composites, potentially unlocking new opportunities for innovation in this field.

Acknowledgements
None declared.

Funding
The authors received no financial support for the research, authorship, and/or publication of this manuscript.

Conflict of Interest
The authors declared no potential conflicts of interest with respect to the research, authorship, and/or publication of this manuscript.

Author Contributions
All of the authors made substantial contributions to conception and design, or acquisition of data, or analysis and interpretation of data; were involved in drafting the manuscript or revising it critically for important intellectual content; and gave final approval of the version to be published.

Data Availability
The datasets created and/or analyzed during the current study are not publicly available, but are available from the corresponding author upon reasonable request.

REFERENCES

Abo-El-Enein S, Abou-Gamra Z, El-Hosiny F, El-Gamal S (1996). Characteristics of lime-silica fume mixtures. *Journal of Thermal Analysis,* 46, 275-284.

Al Zaidi AKA, Demirel B, Atis CD (2019). Effect of different storage methods on thermal and mechanical properties of mortar containing aerogel, fly ash and nano-silica. *Construction and Building Materials,* 199, 501-507.

Alakara E, Sevim Ö, Demir İ, Günel G (2022). Effect of waste concrete powder on slag-based sustainable geopolymer composite mortars. *Challenge Journal of Concrete Research Letters*, 13(3), 101-106.

Al-Amoudi O, Maslehuddin M, Shameem M, Ibrahim M (2007). Shrinkage of plain and silica fume cement concrete under hot weather. *Cement and Concrete Composites,* 29(9), 690-699.

Al-Waked Q, Kinuthia JM, Adeleke BO, Oti J, Khalifa A (2023). Effects of mellowing practice on the strength and swelling properties of road construction materials: Case of sulphate-bearing clay soils stabilised with lime-silica fume blended binder. *Materials,* 16(6), 2187.

Ayasgil D, Ince C, Derogar S, Ball RJ (2022). The long-term engineering properties and sustainability indices of dewatering hydrated lime mortars through Jacaranda seed pods. *Sustainable Materials and Technologies,* 32, e00435.

Bajpai R, Choudhary K, Srivastava A, Sangwan KS, Singh M (2020). Environmental impact assessment of fly ash and silica fume based geopolymer concrete. *Journal of Cleaner Production,* 254, 120147.

Bhutta MAR, Ariffin NF, Hussin MW, Lim NHAS (2013). Sulfate and sulfuric acid resistance of geopolymer mortars using waste blended ash. *Jurnal Teknologi*, 61(3), 1-5.

Calis G, Akpinar ME, Yildizel SA, Çöğürcü MT (2021). Evaluation and optimization Of PVA reinforced cementitious composite containing metakaolin and fly ash. *Revista Romana de Materiale,* 51(1), 53-66.

Çelikten S, Sarıdemir M, Akçaözoğlu K (2020). Effect of calcined perlite content on elevated temperature behaviour of alkali activated slag mortars. *Journal of Building Engineering*, 32, 101717.

Cohen MD, Bentur A (1988). Durability of portland cement-silica fume pastes in magnesium and sodium sulfate solutions. *Materials Journal,* 85(3), 148-157.

Das SK, Mustakim SM, Adesina A, Mishra J, Alomayri TS, Assaedi HS, Kaze CR (2020). Fresh, strength and microstructure properties of geopolymer concrete incorporating lime and silica fume as replacement of fly ash. *Journal of Building Engineering,* 32, 101780.

Duxson P, Provis JL, Lukey GC, Van Deventer JS (2007). The role of inorganic polymer technology in the development of 'green concrete'. *Cement and Concrete Research,* 37(12), 1590-1597.

Gao L, Adesina A, Das S (2021). Properties of eco-friendly basalt fibre reinforced concrete designed by Taguchi method. *Construction and Building Materials,* 302, 124161.

Golafshani EM, Behnood A (2019). Estimating the optimal mix design of silica fume concrete using biogeography-based programming. *Cement and Concrete Composites,* 96, 95-105.

Guleria AN, Salhotra S (2016). Effects of silica fume (micro silica or nano silica) on mechanical properties of concrete: A review. *International Journal of Civil Engineering and Technology,* 7(4), 345-357.

Güney B (2019). Refrakter yalıtım malzemesi üretiminin deneysel olarak araştırılması. *Journal of the Institute of Science and Technology,* 9(2), 880-889.

Jena S, Panigrahi R, Sahu P (2019). Effect of silica fume on the properties of fly ash geopolymer concrete. *Sustainable Construction and Building Materials*, Select Proceedings of ICSCBM 2018.

Kang S-H, Kwon Y-H, Moon J (2019). Quantitative analysis of CO_2 uptake and mechanical properties of air lime-based materials. *Energies,* 12(15), 2903.

Karanafti A, Theodosiou T, Tsikaloudaki K (2022). Assessment of buildings' dynamic thermal insulation technologies-A review. *Applied Energy,* 326, 119985.

Kaya M, Karahan O, Atiş CD (2023). Influence of silica fume additive and activator ratio on mechanical properties in slaked lime-based alkali-activated mortars. *Iranian Journal of Science and Technology, Transactions of Civil Engineering,* 47(2), 873-889.

Koca C (1996). Yüksek performanslı beton üretiminde mikrosilis, curuf, klinker karışımı çimento kullanımı. 4. *Ulusal Beton Kongresi Beton Teknolojisinde Mineral ve Kimyasal Katkılar Bildiri Kitabı,* TMMOB İnşaat Mühendisleri Odası, İstanbul, 381-394.

Kosse P, Blomberg K, Mikola A, Heinonen M, Kuokkanen A, Lange R-L, Lübken M, Wichern M (2016). Climate change and greenhouse gas emissions within the context of urban wastewater management. *Water Solutions,* 2, 89-94.

Liu XH, Lv XD, Fu JX, Peng P, Gai GS (2009). Application of silica fume in China. *Advanced Materials Research,* 58, 21-26.

Mahmoodi O, Siad H, Lachemi M, Dadsetan S, Şahmaran M (2022). Optimized application of ternary brick, ceramic and concrete wastes in sustainable high strength geopolymers. *Journal of Cleaner Production*, 338, 130650.

Malathy R, Shanmugam R, Chung I-M, Kim S-H, Prabakaran M (2022). Mechanical and microstructural properties of composite mortars with lime, silica fume and rice husk ash. *Processes,* 10(7), 1424.

Muller A, Scrivener K, Skibsted J, Gajewicz A, McDonald P (2015). Influence of silica fume on the microstructure of cement pastes: New insights from 1H NMR relaxometry. *Cement and Concrete Research,* 74, 116-125.

Okoye F, Durgaprasad J, Singh N (2016). Effect of silica fume on the mechanical properties of fly ash based-geopolymer concrete. *Ceramics International,* 42(2), 3000-3006.

Oltulu M, Şahin R (2013). Effect of nano-SiO_2, nano-Al_2O_3 and nano-Fe_2O_3 powders on compressive strengths and capillary water absorption of cement mortar containing fly ash: A comparative study. *Energy and Buildings*, 58, 292–301.

Petch H (1961). The hydrogen positions in portlandite, Ca $(OH)_2$, as indicated by the electron distribution. *Acta Crystallographica,* 14(9), 950-957.

Rashad AM, Abd El Fattah AM, Morsi W (2022). Aluminum dross for thermal insulation and acoustic absorption of alkali-activated slag mortars. *ACI Materials Journal,* 119(4), 151-164.

Rashad AM, Gharieb M, Shoukry H, Mokhtar M (2022). Valorization of sugar beet waste as a foaming agent for metakaolin geopolymer activated with phosphoric acid. *Construction and Building Materials,* 344, 128240.

Rashad AM, Mosleh YA, Mokhtar M (2024). Thermal insulation and durability of alkali-activated lightweight slag mortar modified with silica fume and fly ash. *Construction and Building Materials,* 411, 134255.

Rodrigues F, Evangelista L, Brito JD (2013). A new method to determine the density and water absorption of fine recycled aggregates. *Materials Research,* 16, 1045-1051.

Tho-In T, Sata V, Chindaprasirt P, Jaturapitakkul C (2012). Pervious high-calcium fly ash geopolymer concrete. *Construction and Building Materials,* 30, 366-371.

Thokchom S, Ghosh P, Ghosh S (2009). Acid resistance of fly ash based geopolymer mortars. International *Journal of Recent Trends in Engineering*, 1(6), 36.

TS EN 12390-3 (2019). Beton-Sertleşmiş Beton Deneyleri – Bölüm 3: Deney Numunelerinde Basınç Dayanımının Tayini. Turkish Standards Institution, Ankara, Türkiye

TS EN 12390-5 (2019). Beton-Sertleşmiş beton deneyleri – Bölüm 5: Deney Numunelerinde Eğilme Dayanımının Tayini. Turkish Standards Institution, Ankara, Türkiye.

Van Nguyen M (2023). Drivers of innovation towards sustainable construction: A study in a developing country. *Journal of Building Engineering,* 80, 107970.

Wang X, Ding S, Ashour A, Ye H, Thakur VK, Zhang L, Han B (2024). Back to basics: Nanomodulating calcium silicate hydrate gels to mitigate CO_2 footprint of concrete industry. *Journal of Cleaner Production,* 434, 139921.

Yıldızel SA, Çalış G (2019). Design and optimization of basalt fiber added lightweight pumice concrete using taguchi method. *Revista Romana De Materiale/ Romanian Journal of Materials,* 49(4), 544-553.

Yildizel SA, Tayeh B, Uzun M (2022). The evaluation of calcium carbonate added and basalt fiber reinforced roller compacted high performance concrete for pavement. *Case Studies in Construction Materials*, 17, e01293.

Yorulmaz H, Özuzun S, Uzal B, İlkentapar S, Durak U, Karahan O, Atiş C (2021). Effects of dry particle coating with nano- and microparticles on early compressive strength of portland cement pastes. *Challenge Journal of Concrete Research Letters*, 12(4), 125-130.

Zakka W P, Lim NHAS, Khun MC (2021). A scientometric review of geopolymer concrete. *Journal of Cleaner Production,* 280, 124353.